Journal of Volcanology and Geothermal Research 440 (2023) 107872

Contents lists available at ScienceDirect

Journal of Volcanology and Geothermal Research

journal homepage: www.journals.elsevier.com/journal-of-volcanology-and-geothermal-research

Monogenetic scoria cone and associated lava flow volume estimates and their controlling factors

Rong Zhang [a,*], Marco Brenna [a], Gabor Kereszturi [b]

[a] Department of Geology, University of Otago, Dunedin, New Zealand
[b] Volcanic Risk Solutions, School of Agriculture and Environment, Massey University, Private Bag 11 222, Palmerston North, New Zealand

ARTICLE INFO

Keywords:
Monogenetic volcanic field
Scoria cone
Lava flow
Eruptive volume

ABSTRACT

Estimating eruption volumes of volcanoes is crucial for studying the development and evolution of volcanoes and assessing volcanic hazards. Volume estimates for polygenetic volcanoes are well-explored but individual monogenetic volcanoes have received less attention. This could be attributed to the lower perceived hazards resulting from their smaller size and rare eruptive occurrences within volcanic fields. However, accurately determining the volume of individual monogenetic volcanoes is significant for understanding volcanic field development and evolution. Estimates of individual monogenetic eruptions may be challenging due to overlapping lava flows from different vents within a volcanic field or underestimation resulting from the breaching of small-volume scoria cones. This study aims to evaluate the relationship between the morphometric parameters of scoria cones and the volumes of associated lava flows using the globally free Advanced Land Observing Satellite (ALOS) World 3D 30 m (AW3D30) DEM, the US National Elevation Dataset (NED) 10 m DEM, and related satellite images and terrain maps. The results show that the diameter of the scoria cone base (Wco) correlates best with the associated lava flow volume, and Wco is the parameter least affected by later onlapping lava flows. Numerous factors influence the volumes of monogenetic volcanic eruptions. The regional tectonic environment, such as tectonic setting and crust thickness, has been found to control Wco and hence the volume of monogenetic volcanoes. Subduction zones and thicker crust settings are characterized by the most voluminous monogenetic volcanoes. These environments facilitate the accumulation of magma, supporting larger volcanic eruptions. Magma density also correlates with monogenetic eruption volume. Lower density magma is more likely to erupt and form larger monogenetic volcanoes. Furthermore, pre-existing crustal weaknesses such as fault systems are the main factors affecting magma movement in monogenetic shallow plumbing systems and facilitate magma ascent to the surface. Local stresses appear to have a lesser influence on eruptive volumes. Magma source shape has minor influence on monogenetic eruption volumes. Evaluation of all these parameters will provide more robust estimates of potential eruption volumes, hence informing volcanic field hazards assessment.

1. Introduction

Spatially distributed "monogenetic" volcanoes are among the most common and ubiquitous volcanic features on Earth and the terrestrial planets (Wood, 1979). Sensu stricto, monogenetic volcanoes are generally defined as erupting predominantly mafic magma during short-lived eruptions characterized by small eruptive volumes (typically $\leq 1 km^3$) (Németh and Kereszturi, 2015). In a volcanic field or on the flank of a large volcano they usually occur in clusters of spatter cones, scoria (cinder) cones, tuff rings, tuff cones, maars and lava domes, depending on environmental and geologic factors controlling eruption styles (Connor and Conway, 2000; Kereszturi and Németh, 2012; Valentine and Connor, 2015; Murcia and Németh, 2020). Scoria cones are the most common edifice-type in volcanic fields, enabling robust statistical studies of their morphometry (e.g., Favalli et al., 2009; Fornaciai et al., 2012; Uslular et al., 2021; Sieron et al., 2023).

When exploring monogenetic volcanism and its geological hazards, the erupted volume is an overlooked but important parameter. Although lava flows account for the largest proportion of total erupted volume (Wood, 1980; Hasenaka and Carmichael, 1985; Kereszturi et al., 2013), establishing the relationship between lava flows and their associated cone volumes have been challenging due to nested volcanic complexes

* Corresponding author.
E-mail address: cnrongzhang@gmail.com (R. Zhang).

https://doi.org/10.1016/j.jvolgeores.2023.107872
Received 23 February 2023; Received in revised form 10 July 2023; Accepted 12 July 2023
Available online 19 July 2023

with overlapping depositions. Wood (1980) proposed a relationship between the volume of scoria cones and associated lava flows; however, that early model was limited by a small sample size (i.e., only six volcanic fields) and imprecise measurement techniques (e.g., volume calculated as the product of area and average thickness).

With the continuous improvement of Digital Elevation Model (DEM) resolution and the availability of global free DEMs, the extraction of morphometric attributes, including volumes of monogenetic cones (e.g., scoria cones or cinder cones), has become convenient and more precise (Fornaciai et al., 2012; Zhang et al., 2022). Even though there is an increasing interest in volcanic morphology using globally available DEMs (Grosse et al., 2012; Paguican et al., 2021), there is limited research on the factors influencing their eruptive volumes. Eruptive volumes have been inferred to be related to the tectonic environment (Fornaciai et al., 2012) and the distribution of monogenetic volcanoes appear associated with crustal thickness (Mazzarini, 2004, 2007; Mazzarini et al., 2010). Although magmas feeding monogenetic volcanoes originate within the mantle and rise rapidly to the surface in a relatively short period, there is increasing evidence that many of these magmas may have undergone deep or shallow stalling, evolution and mixing/mingling, resulting in petrological diversity (Brenna et al., 2010, 2011, 2018; Erlund et al., 2010; McGee et al., 2011). Nonetheless, the effects of the specific factors, such as tectonic setting, crustal properties and magma properties (composition, density, viscosity), on the eruptive volumes and morphology of monogenetic volcanic edifices are still unclear.

This study utilizes globally available DEMs and multispectral satellite images to assess the relationship between morphometric parameters of scoria cones and the volumes of associated lava flows. Additionally, it investigates the factors influencing eruptive volumes, with a special interest in the correlation of scoria cone morphology with tectonic settings and magma properties.

2. Database and methods

2.1. Database

For this study, we collated a database of a total of 4817 individual scoria cones (Table 1) from thirty-nine monogenetic volcanic fields worldwide (Table 2). These volcanic fields all have young-looking volcanoes formed during the Holocene or Upper Pleistocene, which experienced diverse degrees of erosion that has modified their original morphology.

To establish the volumetric relationship between cones and lava flows, we selected 49 volcanoes from 33 volcanic fields (Tables 1 and 3), which are young-looking and were subjected to no or little erosion. These volcanoes are easily identifiable on satellite imagery by their distinct volcanic cone shapes and the visible outlines of their associated lava flows. >1200 well-preserved volcanic cones from twenty-seven monogenetic volcanic fields were selected to study the tectonic factors influencing monogenetic volcanic size (Table 1 and Supplementary Data 1). To analyze the relationship between magmatic chemical and physical properties and the eruptive volumes, we collected published geochemical data from 62 volcanoes across 22 monogenetic volcanic fields (Table 1 and Supplementary Data 2). Six monogenetic volcanic fields with 1073 volcanoes were selected to study the relationship between eruptive volumes and vent distribution, magma source shapes, local stresses and pre-existing faults (Table 1 and Supplementary Data 3 and 4). We used 3730 volcanic cones from 14 volcanic fields to assess the magma output rate from volcanic fields (Table 1 and Supplementary Data 5).

Table 1
Number of volcanic fields and scoria cones involved in each analysis.

Analysis	Volcanic field	Scoria cones
Total database	39	4817
Cone vs. lava flow relationship	33	49
Tectonic controls	27	1220
Chemical and physical properties	22	62
Spatial distribution and density	6	1073
Magma output rate	14	3730

2.2. Morphometric parameterization

The selected scoria cones and associated lava flows were manually delineated, based on freely available DEM data, terrain maps and satellite images (Fig. 1). Advanced Land Observing Satellite (ALOS) World 3D 30 m (AW3D30) (Tadono et al., 2016) was used in this study to carry out the morphometric parameterization except for the four monogenetic volcanic fields from the United States (Table 2), in which 10 m National Elevation Dataset (NED) (Gesch et al., 2014, 2018) were used. AW3D30 has been robustly assessed for analyzing morphometric parameters of small-volume cones and was found to be the most accurate globally available DEM (Zhang et al., 2022).

The volume of volcanic cones and lava flows were estimated from the space enclosed by the current surface and the pre-eruption surface, modelled by the interpolation of a triangulated irregular network (TIN) function (c.f., Kereszturi et al., 2013). The mean slope angle (S) of the pre-eruption surface was calculated for each selected scoria cones. The erupted volume of a volcanic center including scoria cone and lava flow is defined as:

$$V = \sum \Delta z_i xy \tag{1}$$

where Δz_i is the elevation difference between the current and the pre-eruptive surface at the grid cell i, and x and y are the dimensions of the pixel size along the two main principal directions. Vco and Vla are defined as the volume of volcanic cone and lava flow, respectively.

In this study, the maximum height of volcanic cones (Hco) was quantified following the methods in Favalli et al. (2009), as:

$$Hco = \Delta z_{max} \tag{2}$$

where Δz_{max} is the maximum elevation difference between the crater rim and the pre-eruption surface.

The planimetric areas of volcanic cone bases (Aco) and craters (Acr) were calculated using ArcGIS Pro. Following Favalli et al. (2009), average diameters of the cone base (Wco) and crater (Wcr) were defined as:

$$Wco = 2\sqrt{Aco/\pi} \tag{3}$$

$$Wcr = 2\sqrt{Acr/\pi} \tag{4}$$

2.3. Morphometric parameter analysis

2.3.1. Cone vs. lava flow volumes

To minimize errors, scoria cones and associated lava flow with volumes $>5 \times 10^6$ m^3 and 10×10^6 m^3, respectively, were used for the analysis (Zhang et al., 2022). The 49 selected scoria cones (Table 3) were classified into two categories: breached (Fig. 2a) and intact (Fig. 2b). A breached scoria cone has an open crater, while an intact volcanic cone has a closed crater. For breached scoria cones, the crater and base outlines were extrapolated across the opening from the curved lines of the preserved crater rims and cone bases, respectively (Fig. 2a). This method can reduce the area and diameter errors of craters and bases enlarged by breaching. We used satellite images (e.g., from Maxar, Fig. 1a), terrain maps (e.g., from Esri, NASA, NGA, USGS, Fig. 1b) and published geological maps (e.g., Báez et al., 2017).

2.3.2. Tectonic controls

Kruskal-Wallis H test was used to determine the tectonic factors that

Table 2
Information of monogenetic volcanic fields.

Volcanic field	Location	Dominant rock type	Tectonic setting	Tectonic regime	Crust thickness	Age	Reference
Afar	Eritrea-Ethiopia	Basaltic	Rift	Extension	23–25 km	Late Pleistocene-Holocene	De Fino et al., 1973; Dugda et al., 2005; Teklay et al., 2010
Altiplano-Puna	Chile	Andesitic	Subduction	Extension	70 km	Quaternary	Zandt et al., 2003; González-Maurel et al., 2019
Antofagasta de la Sierra	Argentina	Trachybasalt/Basaltic Trachyandesite	Subduction	Compression	50–60 km	Late Miocene-Holocene	Risse et al., 2008; Báez et al., 2017; Morfulis et al., 2020
Armenia	Armenia	Basaltic Andesite	Intraplate	Strike-Slip	32–35 km	Quaternary	Philip et al., 2001; Karakhanian et al., 2002; Weller et al., 2006; Lin et al., 2020
Auckland	New Zealand	Basaltic	Intraplate	Extension	29 km	Late Pliocene-Holocene	Kereszturi et al., 2013
Calalaste	Argentina	Basaltic to Andesitic	Subduction	Compression	50–60 km	Late Miocene-Holocene	Morfulis et al., 2020
Central Anatolian	Turkey	Basaltic	Intraplate	Strike-Slip	35–40 km	Middle Miocene-Holocene	Gürsoy et al., 1998; Tezel et al., 2013; Uslular et al., 2021
Chichinautzin	Mexico	Basaltic to Dacitic	Subduction	Extension	~45 km	Late Pleistocene-Holocene	Schaaf et al., 2005; Mazzarini et al., 2010; Arce et al., 2015
Chyulu Hills	Kenya	Basalt/Basanite	Rift	Extension	40 km	Quaternary	Späth et al., 2000; Dugda et al., 2005; Scoon, 2018
Colima	Mexico	Andesitic	Subduction	Extension	~32 km	Pleistocene	Wallace and Carmichael, 1999; Carmichael et al., 2006
Davis Lake	United States	Andesite	Subduction	Extension	44–46 km	Holocene	Stanley et al., 1990; USGS, n.d.
Fuji	Japan	Basalt	Subduction	Compression	~35 km	Holocene	Ishizuka et al., 2007; Katsumata, 2010; Aoki et al., 2019
Harra of Arhab	Yemen	Basaltic	Intraplate	Extension	~35 km	Quaternary	Neumann van Padang, 1963; Hughes and Collings, 2000; Ahmed et al., 2013; Al-Fakih and Li, 2018
Harras of Dhamar	Yemen	Basaltic	Intraplate	Extension	~35 km	Quaternary	Neumann van Padang, 1963; Hughes and Collings, 2000; Ahmed et al., 2013; Al-Fakih and Li, 2018
Harrat Kishb	Saudi Arabia	Alkali Basalt	Intraplate	Extension	~30 km	Quaternary	Camp et al., 1992; Ahmed et al., 2016
Harrat Lunayyir	Saudi Arabia	Alkali Basalt	Intraplate	Extension	38–43 km	Late Cenozoic	Badri, 1991; Duncan and Al-Amri, 2013
Harrat Rahat	Saudi Arabia	Alkali Basalt	Intraplate	Extension	~38 km	Late Cenozoic	Kereszturi et al., 2016; Tang et al., 2016; Downs et al., 2019
Hualalai	Hawaii	Basalt	Intraplate	Extension	<15 km	Late Pleistocene-Holocene	Moore and Clague, 1991; Hammer et al., 2006
Jeju Island	South Korea	Alkaline basalt to Trachyte	Intraplate	Extension	~35 km	Early Pleistocene-Holocene	Brenna et al., 2015
Kamchatka	Russia	Basalt to Basaltic Andesite	Subduction	Extension	38–40 km	Late Pleistocene-Holocene	Levin et al., 2002; Ponomareva et al., 2007; Dirksen and Bazanova, 2010
Kamo	Japan	Basalt	Subduction	Extension	24 km	Late Pleistocene-Holocene	Nche et al., 2021
Kula	Turkey	Basaltic	Intraplate	Extension	~30 km	Quaternary	Alıcı et al., 2002; Tezel et al., 2013; Heineke et al., 2016
La Palma	Canary Islands	Basalt	Intraplate	Extension	<15 km	Quaternary	HernandeÁz-Pacheco and Valls, 1982; Guillou et al., 1998, 2001; Day et al., 1999
Lamongan	Indonesia	Basalt	Subduction	Extension	~35 km	Holocene	Carn, 2000; Carn and Pyle, 2001; Bahri et al., 2021
Las Pilas-El Hoyo	Nicaragua	Basaltic	Subduction	Extension	~33 km	Holocene	Roggensack, 2001; La Femina et al., 2004
Longgang	China	Basaltic	Intraplate	Compression	~38 km	Neogene-Quaternary	Duan et al., 2005; Zhao et al., 2021
Meidob	Sudan	Basanite	Intraplate	Strike-Slip	33–37 km	Late Cenozoic	Franz et al., 1997; El Tahir et al., 2013
Michoacán-Guanajuato	Mexico	Basaltic	Subduction	Extension	~38 km	Late Pleistocene-Holocene	Mazzarini et al., 2010
Negro Peinado	Argentina	basaltic to andesitic	Subduction	Compression	50–60 km	Late Miocene-Holocene	Morfulis et al., 2020
Newer	Australia	Basalt	Intraplate	Compression	31 km	Pliocene-Holocene	Hill et al., 1995; Lesti et al., 2008; van den Hove et al., 2017
Northern Lake Abaya	Ethiopia	Basalt to Rhyolitic	Rift	Extension	~30 km	Late Miocene-Holocene	Dugda et al., 2005; Chernet, 2011
Payenia	Argentina	Basaltic	Subduction	Compression	40–60 km	Quaternary	McGlashan et al., 2008; Søager et al., 2013; May et al., 2018
Puebla Valley	Mexico	Andesite	Subduction	Extension	~45 km	Late Pleistocene-Holocene	Schaaf et al., 2005
San Francisco	United States	Basaltic to Andesitic	Intraplate	Extension	35–40 km	Late Miocene-Holocene	Aldrich Jr and Laughlin, 1984; Gilbert et al., 2007; Fenton and Niedermann, 2014
Southwestern Nevada	United States	Basaltic	Intraplate	Extension	~36 km	Pliocene-Quaternary	Heizler et al., 1999; Valentine et al., 2007; Schulte-Pelkum et al., 2011
Springerville	United States	Basalt	Intraplate	Extension	~35 km	Pliocene-Pleistocene	Condit et al., 1989; Gilbert et al., 2007

(continued on next page)

Table 2 (*continued*)

Volcanic field	Location	Dominant rock type	Tectonic setting	Tectonic regime	Crust thickness	Age	Reference
Tenerife	Canary Islands	Basanite to Phonolite	Intraplate	Extension	<15 km	Late Miocene-Holocene	Carracedo et al., 2007; Kröchert and Buchner, 2009; Di Roberto et al., 2020; Risica et al., 2020
Todra	Niger	Basaltic/Trachytic/Phonolitic	Intraplate	Extension	42–44 km	Oligocene-Holocene	Liégeois et al., 2005; Yacouba and Glaznev, 2021
Wudalianchi	China	Alkaline Basaltic	Intraplate	Extension	~32 km	Neogene-Quaternary	Tao et al., 2014; Zhao et al., 2014

have a statistically significant influence on scoria cone morphological parameters that are not normally distributed, such as Wco (Supplementary Fig. 1). The test can indicate the strength of the relationships between the parameters and categorical tectonic factors (Davis, 2002). The p-values calculated by the test allowed determining if the medians of the parameters within each class were statistically similar or different than the ones within the other classes. A p-value below 0.05 meant that the compared classes are statistically different.

2.3.3. Chemical composition

Less evolved and more evolved volcanoes are distinguished by their geochemical characteristics (see Supplementary Data 2). Evolution in this context refers to the degree of magmatic differentiation, as well as the overall variability of compositions within a single volcano. If rock samples from a volcano show complex geochemical and rock type variations and ranges, the volcano is defined as more evolved, such as the La Poruña volcano (e.g., González-Maurel et al., 2019). If samples from a volcano instead show a single rock composition and have less variable geochemical characteristics, the volcano is defined as less evolved, such as the Alumbrera volcano (e.g., Báez et al., 2017). This approach is sensitive to the number of samples available for each volcano, but was chosen to understand the impact of each individual volcano's geochemical variation on its volume. Spearman's correlation coefficients can provide the correlation strength between non-normally distributed chemical compositions and morphological parameters of scoria cones (Schober et al., 2018).

2.3.4. Physical parameters

To estimate the density (ρ) and viscosity (η) of magma, we first calculate the temperatures of the magmatic liquids at atmospheric pressure using Petrolog3 (Danyushevsky and Plechov, 2011), assuming that the whole rock compositions represent the melts. The densities were then estimated by DensityX (Iacovino and Till, 2019) at the estimated temperatures and atmospheric pressure. The viscosities of the melts were calculated following the method of Giordano et al. (2008).

2.3.5. Spatial distribution and density

To explore the relationship of vent clusters to the size of monogenetic volcanoes, each of the six selected volcanic fields was subdivided into clusters using the Kernel Density tool of the ArcGIS Pro software (c.f., van den Hove et al., 2017). Clusters at different search radii may be spatially correlated with magma at different levels in the crust or mantle, i.e., vent cluster maps with large search radii may reflect deep spatial correlations, while the maps with short search radii may reveal shallow spatial correlations (Connor, 1990). The search radius was specified as 2–3 times the average minimum distance between vents within each volcanic field, which allows the clusters to reflect small, i.e., local-scale, magma eruption models (Mazzarini, 2007).

We further analyzed the relationship between the vent alignments and ellipse long axes of six selected volcanic fields and the sizes of their scoria cones. The minimum enclosing ellipses of the volcanic fields were derived with the function getMinEllipse of the package 'shotGroups' in the R software (Wollschlaeger, 2022). The MATLAB tool of Thomson and Lang (2016) was designed depending on the two-point azimuth method of Lutz (1986) and the modified two-point azimuth method of Cebriá et al. (2011) to investigate vent alignments. The method of Lutz (1986) determines all pairs of features and provides peaks of the histogram as preferred alignments. To eliminate the resulting dependence of the area shape present in the Lutz (1986) method, the raw histogram was normalized by Monte Carlo simulations of random patterns with the same number of points and similar spatial extent. The method determines a confidence level (95%) above which peaks are considered significant. In the method of Cebriá et al. (2011), azimuths are only calculated between features within the minimum significant distance, d_{ms}. This distance d_{ms} is equal to $|x - 1\sigma|/3$, where x is the mean separation distance and σ is the standard deviation. We employed the two methods and combined previous studies, and then manually selected major alignments connected by at least three vents to analyze the relationship between the major alignments and the distribution of volcano sizes.

3. Results

3.1. Volumetric relationship between scoria cones and associated lava flows

Vco, Wco, Hco and Wcr are scale-dependent morphometric parameters for cone-shaped volcanoes formed by the tephra accumulation from the eruption column via turbulent jets and ballistic ejection (McGetchin et al., 1974; Kereszturi and Németh, 2012). Porter (1972) and Wood (1980) proposed the Hco/Wco value of 0.18 and the Wcr/Wco value of 0.40 for the "ideal" scoria cone. However, the morphometric parameters often deviate from the symmetrically perfect cones due to the inclination of pre-eruption surface (e.g., Kereszturi et al., 2012), magma effusion from crater and erosion (e.g., Kervyn et al., 2012), making morphometric parameters not independently relatable to real cone volume.

Our dataset (e.g., Hco/Wco and Wcr/Wco) fall within the data range of Fornaciai et al. (2012), representing the global cone population (Fig. 3a). The overall ratios of breached cones compared to intact cones are clearly distinct (Fig. 3a), whereas there is no apparent distinction between younger (≤2.5 ka) and "older" cones (>2.5 ka), neither between cones erupted on flat or steep pre-eruption surfaces (Fig. 3b and c). These relationships suggest that magma effusion from the crater was the main cause of the variation in the cone shape, whereas inclination of pre-eruption surface or erosion has not played a significant role in the morphologies of the studied cone population at 30 m scale. The crater of breached cones is significantly widened (Fig. 3d), though the height and base width are moderately affected (Fig. 3e).

The four morphological parameters (Vco, Wco, Wcr, and Hco) of the scoria cones are correlated with the volume of their associated lava flows (Fig. 4). Among these, Wco and Hco has the better correlation ($R^2 = 0.79$ and $R^2 = 0.70$, respectively) with lava flow volume, whereas Wcr has the worst correlation ($R^2 = 0.30$). The relationships between Wco and Hco with Vla are defined by:

$$Vla = 10.32e^{0.003Wco} \quad (5)$$

$$Vla = 11.89e^{0.02Hco} \quad (6)$$

The strong correlation improves ($R^2 = 0.94$ and $R^2 = 0.89$ for Wco

Table 3
List of edifices for analyzing the relationship between scoria cone morphometric and associated lava flow volume.

No.	Volcano name	Volcanic field	Lat (deg)	Long (deg)	Age	Breach	Vco (10^6 m^3)	Vla (10^6 m^3)	Wcr (m)	Hco (m)	Wco (m)	Hco/Wco	Wcr/Wco	S (°)	Reference
1	Unnamed	Afar	13.002	42.582	Holocene	No	19.11	26.05	209	140	760	0.18	0.28	9.53	De Fino et al., 1973
2	Unnamed	Afar	11.816	40.242	Holocene	Yes	10.10	72.56	399	61	784	0.08	0.51	1.57	De Fino et al., 1973
3	La Poruña	Altiplano-Puna	−21.893	−68.500	100 ka	No	37.77	503.32	267	159	875	0.18	0.31	3.59	González-Maurel et al., 2019
4	Alumbrera	Antofagasta de la Sierra	−26.148	−67.385	Holocene	No	90.00	378.28	401	216	1266	0.17	0.32	3.38	Báez et al., 2017
5	Unnamed	Antofagasta de la Sierra	−26.474	−67.466	Pleistocene-Holocene	No	227.50	2770.55	461	298	1802	0.17	0.26	5.62	Báez et al., 2020
6	Unnamed	Armenia	39.723	46.007	4.72 ka	Yes	0.33	54.35	130	21	238	0.09	0.55	5.80	Karakhanian et al., 2002
7	Mt. Eden	Auckland	−36.877	174.764	28.4 ka	No	29.72[a]	109.59[a]	179[a]	127[a]	717[a]	0.18	0.25	0.15	Kereszturi et al., 2013
8	Mt. Mangere[f]	Auckland	−36.950	174.783	22.1 ka	No	34.90[a]	40.78[a]		84[a]	1055[a]	0.08		1.40	Kereszturi et al., 2013
9	Mt. Wellington	Auckland	−36.893	174.846	10.5 ka	No	15.08[a]	99.17[a]	240[a]	111[a]	579[a]	0.19	0.41	1.84	Kereszturi et al., 2013
10	Unnamed	Calalaste	−26.004	−67.799	Late Miocene-Holocene	Yes	17.90	37.30	296	122	875	0.14	0.34	8.39	Morfulis et al., 2020
11	Kucukmedet Tepe	Central Anatolian	37.659	33.631	Holocene	No	93.03	275.17	394	211	1280	0.16	0.31	3.85	Gürsoy et al., 1998
12	Jumento	Chichinautzin	19.209	−99.314	2.032 ka	Yes	21.32	80.29	339	129	822	0.16	0.41	5.29	Arce et al., 2015
13	Pelagatos	Chichinautzin	19.093	−98.962	>2.5 ka; <14 ka	Yes	0.97	73.64	79	38	339	0.11	0.23	7.20	Agustín-Flores et al., 2011
14	Cerro del Agua	Chichinautzin	19.090	−98.989	>2.5 ka; <14 ka	Yes	42.38	242.87	329	165	945	0.18	0.35	9.54	Agustín-Flores et al., 2011
15	Shaitani	Chyulu Hills	−2.873	37.994	1865–6 CE	Yes	12.33	25.97	193	121	620	0.20	0.31	6.53	Scoon, 2018
16	Chaimu	Chyulu Hills	−2.957	38.084	1865–6 CE	Yes	3.20	12.17	139	61	423	0.14	0.33	4.01	Scoon, 2018
17	Apaxtepec	Colima	19.632	−103.493	62 ka	No	10.02	84.76	253	92	714	0.13	0.35	3.21	Carmichael et al., 2006
18	Unnamed	Davis Lake	43.526	−121.811	5.05–5.6 ka	Yes	3.69	180.28	231	86	499	0.17	0.46	8.55	USGS, n.d.
19	Unnamed	Davis Lake	43.482	−121.813	5.05–5.6 ka	No	1.59	111.79	146	42	344	0.12	0.42	3.30	USGS, n.d.
20	Djebel Zebib	Harra of Arhab	15.590	44.114	200 CE	No	26.74	47.29	314	153	887	0.17	0.35	4.60	Hughes and Collings, 2000
21	Unnamed	Harras of Dhamar	14.521	44.727	Quaternary	Yes	9.43	42.93	275	88	784	0.11	0.35	7.24	Ahmed et al., 2013
22	Jabal Hil	Harrat Kishb	22.911	41.335	Holocene	No	56.30	715.65	551	149	1301	0.11	0.42	6.37	Ahmed et al., 2016
23	Unnamed	Harrat Lunayyir	25.149	37.829	Quaternary	Yes	36.31	224.00	334	183	872	0.21	0.38	4.72	Duncan and Al-Amri, 2013
24	Al-Madinah[g]	Harrat Rahat	24.350	39.773	1256 CE	No/Yes	23.00[b]	392.00[b]							Kereszturi et al., 2016
25	Unnamed cone (v5d c3.5)	Hualalai	19.710	−155.840	1.5–3 ka	Yes	0.80	61.57	165	31	377	0.08	0.44	15.74	Moore and Clague, 1991
26	Veer	Kamchatka	53.752	158.448	470 CE	Yes	3.17	12.49	141	71	420	0.17	0.34	9.81	Dirksen and Bazanova, 2010
27	Karadivlit Tepe	Kula	38.576	28.548	3.3 ka	No	19.34	97.17	246	127	702	0.18	0.35	3.72	Heineke et al., 2016
28(1)	Divlit Tepe (1)	Kula	38.621	28.428	0.7–2.5 ka	No	35.31[c]	39.57[c]	246	139	720	0.19	0.34	4.18	Heineke et al., 2016
28(2)	Divlit Tepe (2)	Kula	38.621	28.428	0.7–2.5 ka	No			213	80	510	0.16	0.42	4.18	Heineke et al., 2016
28(3)	Divlit Tepe (3)	Kula	38.621	28.428	0.7–2.5 ka	No			60	25	155	0.16	0.39	4.18	Heineke et al., 2016
29	Montana Quemada	La Palma	28.625	−17.840	1470–92 CE	Yes	15.95	14.08	267	133	735	0.18	0.36	9.45	HernandeÂz-Pacheco and Valls, 1982
30	G. Kendeng	Lamongan	−7.971	113.275	Holocene	Yes	0.58	13.35	96	33	259	0.13	0.37	4.00	Carn and Pyle, 2001
31	Cerro Negro	Las Pilas-El Hoyo	12.506	−86.702	1850–1999 CE	Yes	51.24	49.28	376	188	1006	0.19	0.37	7.15	La Femina et al., 2004
32	Dayizishan	Longgang	42.379	126.201	71 ka	Yes	52.03	1361[d]	552	148	1048	0.14	0.53	1.78	Yu et al., 2005
33	Unnamed	Meidob	15.464	26.365	Holocene	Yes	28.63	162.04	484	130	974	0.13	0.50	2.48	Franz et al., 1997
34	Volcán La Mina	Michoacán-Guanajuato	19.714	−101.433	7 ka	Yes	73.95	575.13	386	200	1144	0.17	0.34	7.08	Kshirsagar et al., 2015
35	Cerro El Zoyate	Michoacán-Guanajuato	19.145	−101.618	6 ka	No	59.17	106.97	407	160	1099	0.15	0.37	7.74	Guilbaud et al., 2012

(*continued on next page*)

Table 3 (*continued*)

No.	Volcano name	Volcanic field	Lat (deg)	Long (deg)	Age	Breach	Vco (10^6 m^3)	Vla (10^6 m^3)	Wcr (m)	Hco (m)	Wco (m)	Hco/ Wco	Wcr/ Wco	S (°)	Reference
36	Cerro La Taza	Michoacán-Guanajuato	19.526	−101.725	8.43 ka	No	23.30	46.39	190	148	755	0.20	0.25	6.12	Hasenaka and Carmichael, 1985
37	Volcán Paricutin	Michoacán-Guanajuato	19.493	−102.252	1943–52 CE	No	68.37	440.08	257	208	1136	0.18	0.23	4.18	Pioli et al., 2008
38	Cerro El Jabali	Michoacán-Guanajuato	19.449	−102.112	3.83 ka	No	55.01	148.64	300	179	1054	0.17	0.28	8.60	Hasenaka and Carmichael, 1985
39	Unnamed	Negro Peinado	−26.480	−68.148	Late Miocene-Holocene	Yes	45.43	91.07	338	210	964	0.22	0.35	6.90	Morfulis et al., 2020
40	Unnamed	Negro Peinado	−26.419	−68.025	Late Miocene-Holocene	Yes	69.63	148.81	506	177	1232	0.14	0.41	5.62	Morfulis et al., 2020
41	Unnamed	Northern Lake Abaya	6.760	37.974	Holocene	No	1.49	19.65	127	38	338	0.11	0.37	6.36	Chernet, 2011
42	Santa Maria[f]	Payenia	−36.301	−69.321	1.99 ka	Yes	25.49	731.32		136	808	0.17			May et al., 2018
43	SP Crater	San Francisco	35.583	−111.631	70 ka	No	79.50	347.81	371	211	1195	0.18	0.31	9.26	Fenton and Niedermann, 2014
44	Lathrop Wells	Southwestern Nevada	36.690	−116.511	80 ka	No	18.58	36.32	191	120	739	0.16	0.26	4.78	Heizler et al., 1999
45	Arafo	Tenerife	28.340	−16.461	1705 CE	Yes	5.30	18.34	279	67	580	0.12	0.48	9.40	Risica et al., 2020
46	Garachico	Tenerife	28.317	−16.764	1706 CE	Yes	4.41	44.66	314	67	592	0.11	0.53	5.71	Risica et al., 2020
47	Unnamed	Todra	17.554	8.464	Holocene	No	6.32	134.02	160	73	686	0.11	0.23	1.77	Liégeois et al., 2005
48	Huoshaoshan	Wudalianchi	48.738	126.154	1721 CE	Yes	6.16	537.38[e]	376	65	709	0.09	0.53	3.81	Zhao et al., 2014
49	Laoheishan	Wudalianchi	48.715	126.118	1719 CE	No	60.71		371	150	1245	0.12	0.30	3.02	Zhao et al., 2014

Vco = Cone volume, Vla = Lava flow volume, Wcr = Crater width, Hco = Cone height, Wco = Cone base width, and S=Slope angle of pre-eruption surface.

[a] Data are cited from Kereszturi et al., 2013.

[b] Data are cited from Kereszturi et al., 2016.

[c] Vco and Vla of Divlit Tepe are the total volume of three volcanic cones.

[d] Data are cited from Yu et al., 2004.

[e] Vla of Huoshaoshan and Laoheishan is estimated as a total.

[f] Multiple craters exist in one volcanic cone.

[g] Multiple cones are associated with one lava flow.

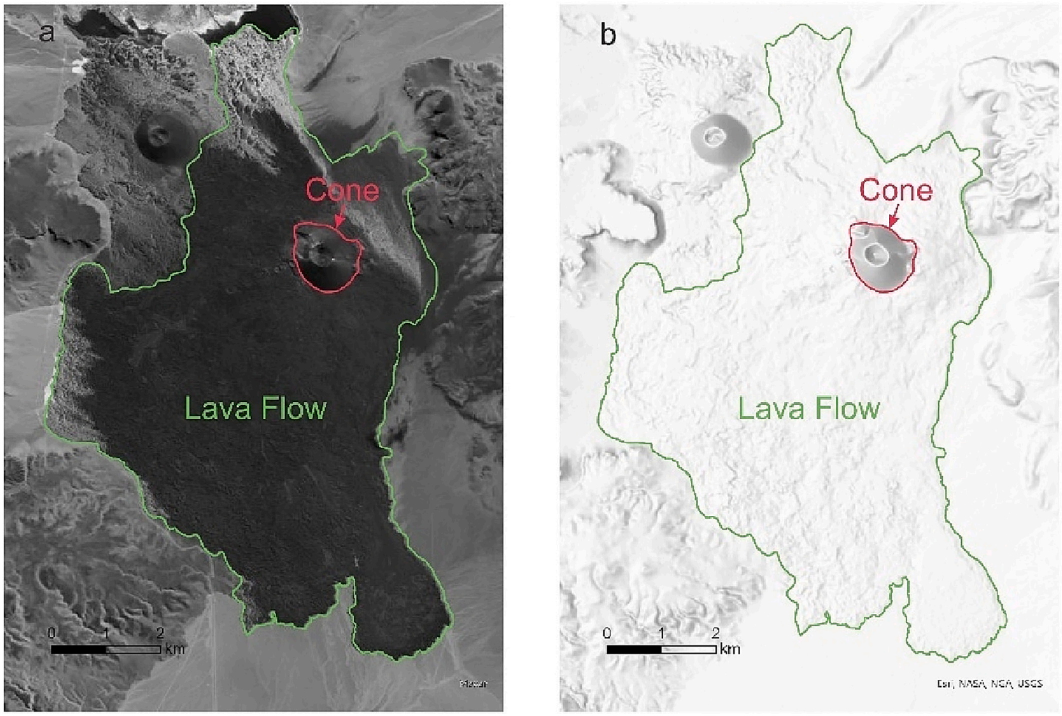

Fig. 1. Cone and lava flow of Alumbrera volcano (Antofagasta de la Sierra Volcanic Field, Argentina) delineated on Maxar satellite image (a), and shaded terrain models from Esri/NASA/NGA/USGS (b).

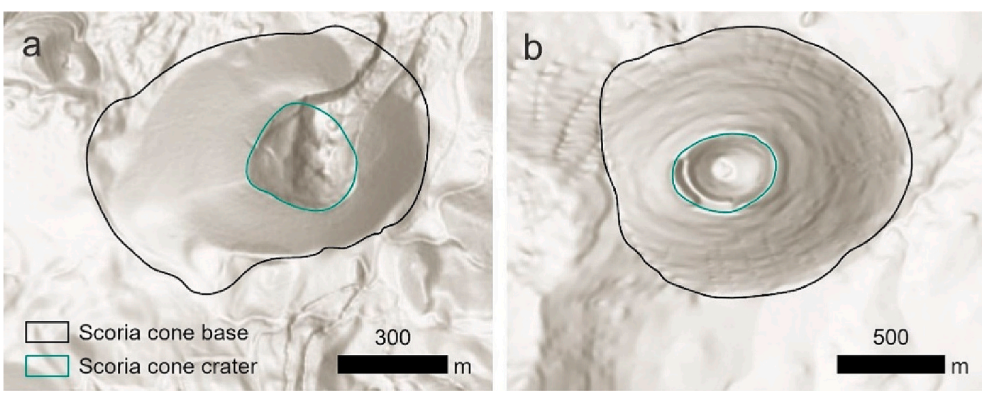

Fig. 2. Classification examples of breached scoria cone (Montana Quemada, La Palma, Canary Islands) (a) and intact scoria cone (SP Crater, San Francisco Volcanic Field, United States) (b). Terrain maps from Esri, NASA, NGA, USGS.

and Hco, respectively) if only intact cones were considred. The relationships between Wco and Hco with Vla for intact scoria cones are given by:

$$Vla = 11.72e^{0.003Wco} \tag{7}$$

$$Vla = 13.14e^{0.02Hco} \tag{8}$$

Furthermore, Wco is probably the parameter least affected by morphological changes (Pérez-López et al., 2011), it also correlates strongly with the volumes of the associated lava flows. The measurement error of Wcr may be large and considerably affected by lava flow breach, flank collapse, e.g., Cumbre Vieja volcano, La Palma, Canary Islands (Day et al., 1999), intermittent eruptions or environmental factors such as wind (e.g., Kereszturi and Németh, 2012), explaining the poor correlation between Wcr and Vla (Fig. 4a).

For all the observed trends among morphometric parameters, we observe no significant distinction based on composition (see Supplementary Data 2), suggesting that the evolution of magma has no special effect on the volume ratio of the scoria cones and the associated lava flows (Fig. 4).

3.2. Relationship between tectonic processes and eruptive volumes

Given the relationship determined above, we consider Wco as the geomorphological parameter that best represents the relationship between scoria cone and associated lava flow volumes. However, Wco shows variations across volcanic fields (Fig. 5a). Volcanic fields with significantly larger and broadly distributed Wco values are Altiplano-Puna, Las Pilas-El Hoyo and Negro Peinado (Fig. 5a). They all occur in subduction tectonic settings, although their tectonic regimes and crust thickness are different (Table 2). On the other hand, Northern Lake Abaya has the smallest Wco (Fig. 5a), and it is located in an extensional tectonic regime with a thinner crust, suggesting a relationship between cone volumes and tectonic/crustal settings. Our analysis suggests that convergent tectonic settings are more favorable for producing larger monogenetic volcanoes compared to extensional tectonic settings,

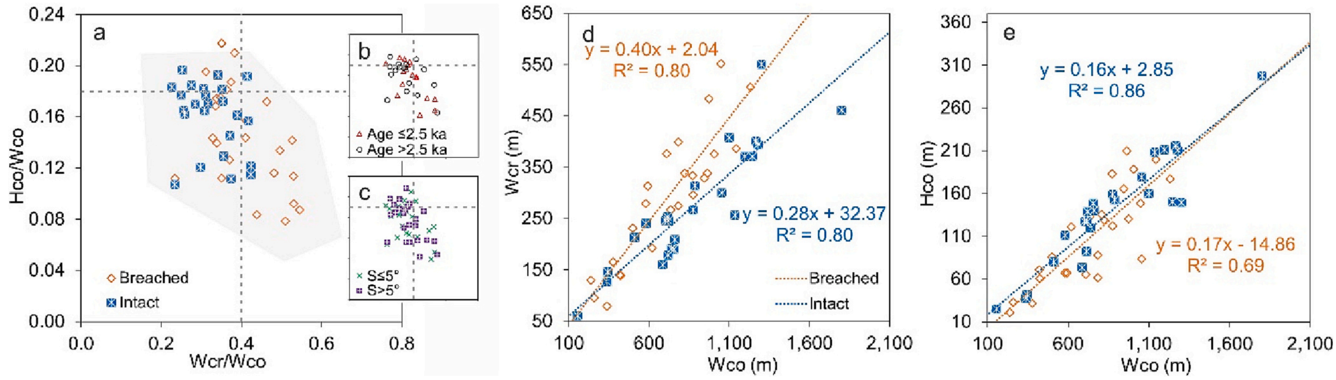

Fig. 3. (a) Plot of Hco/Wco vs. Wcr/Wco. Gray dash lines indicate the "ideal" cone values taken from Porter (1972) and Wood (1980). Gray area refers to the data from Fornaciai et al. (2012). (b–c) The inset shows the same graph as (a) but classified by age (b) and pre-eruptive surface inclination (c). (d) Plot of Wcr vs. Wco. (e) Plot of Hco vs. Wco. Orange and blue dash lines refer to linear trend lines for breached and intact scoria cones, respectively. Wcr = Crater width, Hco = Cone height, Wco = Cone base width, and S=Slope angle of pre-eruption surface. (For interpretation of the references to colour in this figure legend, the reader is referred to the web version of this article.)

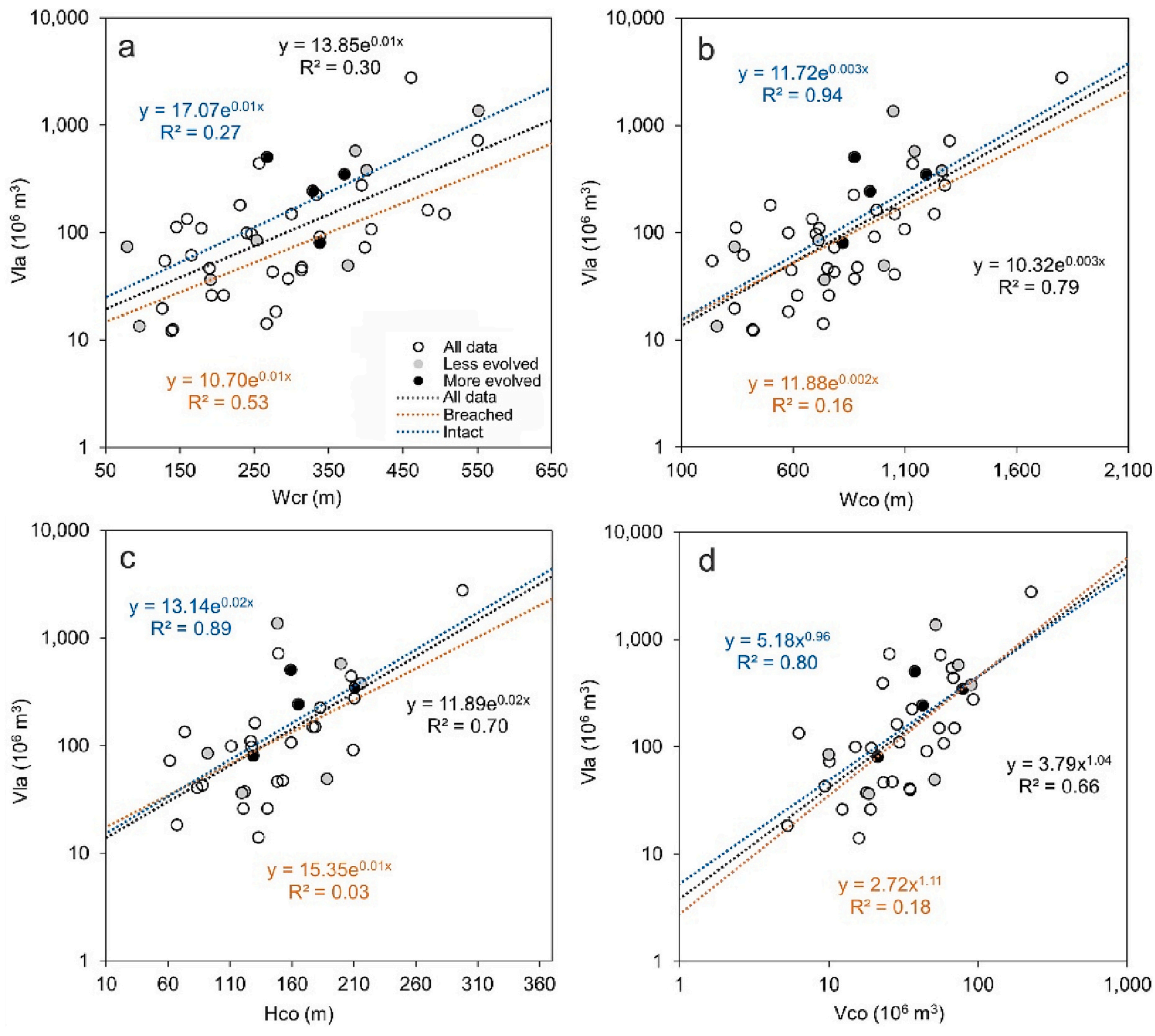

Fig. 4. Scatter plots of cone morphometry vs. associated lava flow volume. (a–c) Plots of Wcr, Wco and Hco vs. Vla. Dash lines are exponential trend lines. (d) Plots of Vco vs. Vla. Black, orange and blue dash lines are power trend lines of all data, breached and intact cones, respectively. Vco = Cone volume, Vla = Lava flow volume, Wcr = Crater width, Hco = Cone height, and Wco = Cone base width. (For interpretation of the references to colour in this figure legend, the reader is referred to the web version of this article.)

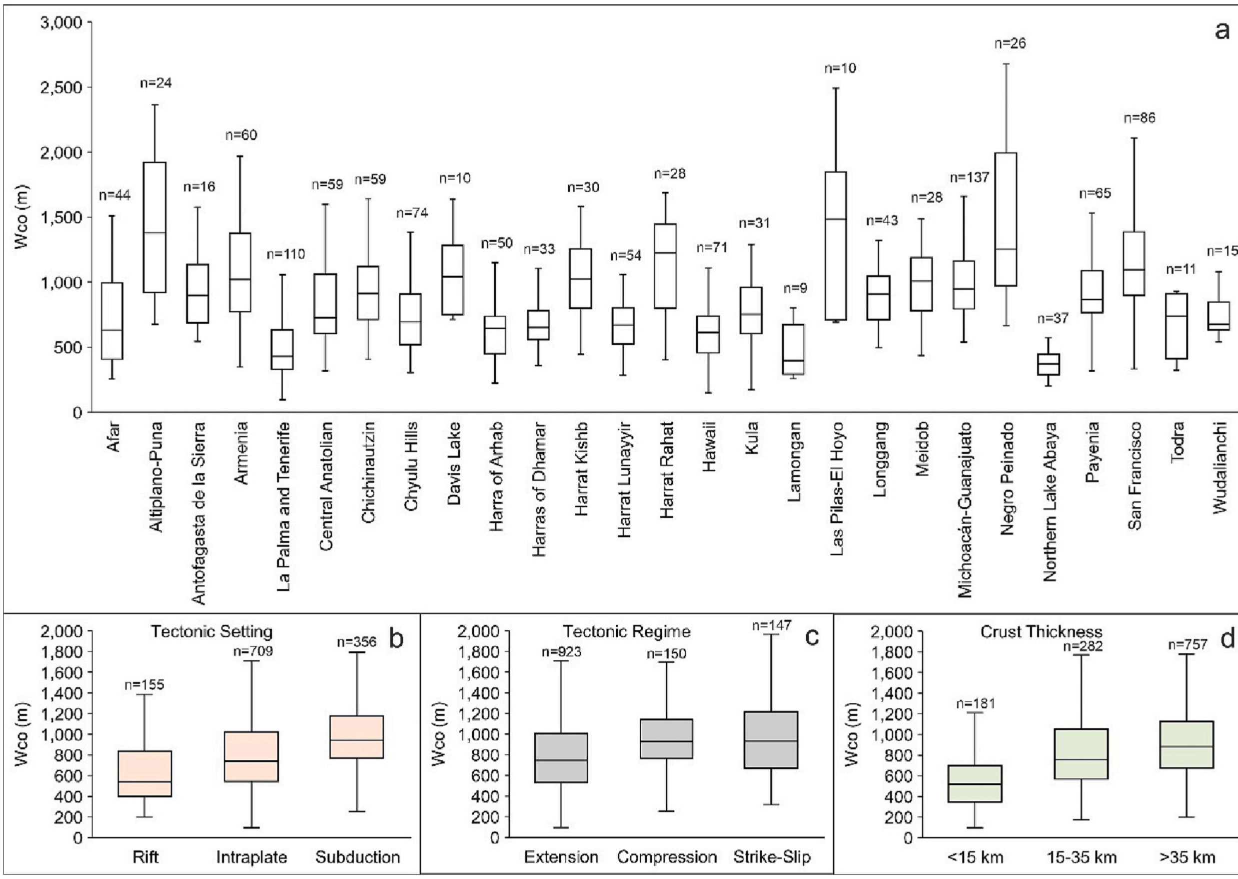

Fig. 5. (a) Boxplot of Wco in the selected 27 volcanic fields. (b) Boxplot of Wco by tectonic setting. (c) Boxplot of Wco by tectonic regime. (d) Boxplot of Wco by crust thickness. Wco = Cone base width.

consistent with the former being the site of most large volcanoes (Sigurdsson et al., 2015; Schmidt et al., 2022).

The Kruskal-Wallis H test ($p < 0.05$) found a statistically significant variation in each pair of classes of tectonic setting, tectonic regime and crust thickness, except for the pair strike-slip and compression ($p = 1.000$) (Table 4). This is illustrated by boxplots (Fig. 5b–d) showing that the subclasses within both tectonic settings and crustal thickness are significantly different, whereas the three tectonic regimes are moderately different. This indicates global tectonic factors, i.e., tectonic setting and crust thickness, strongly influence Wco, while tectonic regime exerts only localized controls that moderately affects Wco. This aligns well with previous studies (e.g., Fornaciai et al., 2012).

Table 4
Kruskal-Wallis H test on the three tectonic processes influencing cone base width. By comparing the similarities between the factors in each tectonic process, the degree of influence of the tectonic process on cone base width is analyzed.

Tectonic processes	Compared class 1	Compared class 2	Adjusted *p*-value[a,b]
Tectonic setting	Rift	Intraplate	0.000
	Rift	Subduction	0.000
	Intraplate	Subduction	0.000
Tectonic regime	Extension	Strike-Slip	0.000
	Extension	Compression	0.000
	Strike-Slip	Compression	1.000
Crust thickness	<15 km	15–35 km	0.000
	<15 km	>35 km	0.000
	15–35 km	>35 km	0.000

[a] Significance values have been adjusted by the Bonferroni correction for multiple tests.
[b] Asymptotic significances (2-sided tests) are displayed. The significance level is 0.05.

3.3. Relationship between magma chemical and physical properties and monogenetic volcano size

The relationship between the magma composition and eruption volume can be explored through the correlation analysis between Wco and the major element compositions from scoria cones (Fig. 6a–i). SiO_2 and Na_2O have a statistically significant positive correlation with Wco, whereas CaO and FeOt have a negative correlation with Wco (Table 5). Of the two volcanic fields with the most abundant geochemical data (Chichinautzin and Tenerife), their compositional trends are consistent with the overall data. Although K_2O, Al_2O_3, MgO and TiO_2 are not significantly correlated with Wco in the overall data, they have consistent trends if considering variability within these two volcanic fields. This can indicate that variability in these four elements may be related to specific magmatic generation processes (e.g., Brenna et al., 2021) that impose variable starting compositions, such as heterogeneities in source lithology. Correlation analysis indicates that the abundances of SiO_2, CaO, NaO, FeOt, TiO_2 and K_2O are significantly correlated with the eruption volume of scoria cones. This suggests that the magma composition is an important factor affecting output volumes (Table 5).

Considering melt density and viscosity calculated from whole-rock chemical compositions, it is apparent that Wco has a negative correlation with melt density, whereas the relationship between melt viscosity and Wco is not obvious, but it could suggest a positive correlation with Wco if considering only individual volcanic fields (Fig. 6j and k). This suggests that magma buoyancy can be one of the main factors controlling Wco, and consequently, eruptive volumes within volcanic fields. Mafic rocks such as basanite and basalt correspond to smaller volcanic

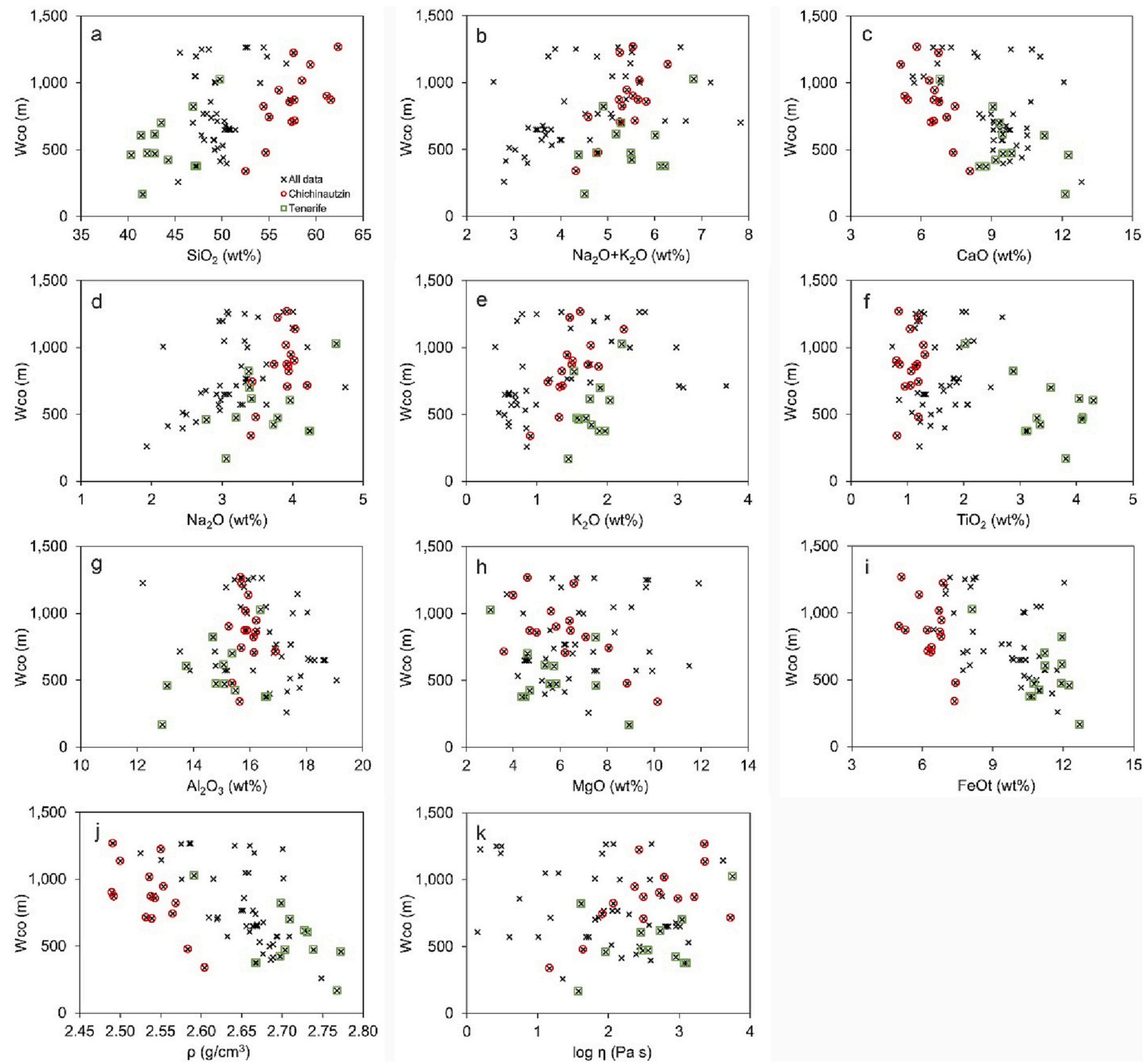

Fig. 6. X-Y plots of scoria cone chemical elements and physical parameters vs. Wco. Wco = Cone base width.

Table 5
Spearman's correlation coefficients between Wco and chemical elements. Data from 69 samples from 62 scoria cones.

		SiO_2	CaO	Na_2O	FeOt	K_2O	TiO_2	Al_2O_3	MgO
Wco	Correlation coefficient	0.397[a]	−0.525[a]	0.344[a]	−0.538[a]	0.361[a]	−0.283[b]	−0.042	0.088
	Sig. (2-tailed)	0.001	0.000	0.004	0.000	0.002	0.018	0.732	0.473
	Number	69	69	69	69	69	69	69	69

Wco = Cone base width.
[a] Correlation is significant at the 0.01 level (2-tailed).
[b] Correlation is significant at the 0.05 level (2-tailed).

sizes, whereas intermediate rocks such as andesite occur in larger volcanoes (Fig. 7).

3.4. Distribution and alignment of monogenetic volcano size

The spatial-volumetric distribution of cones within volcanic fields shows that volcanoes with similar volumes tend to cluster closer together (Fig. 8). For example, volcanoes in clusters 9, 11, 13 and 15 in Longgang volcanic field predominantly contain larger-volume cones, while in clusters 3, 5, 7 and 8 there are mostly small volume cones (Fig. 8c and i). Fig. 8g–l report the size variability in each of the defined clusters for the six selected volcanic fields and illustrate that although

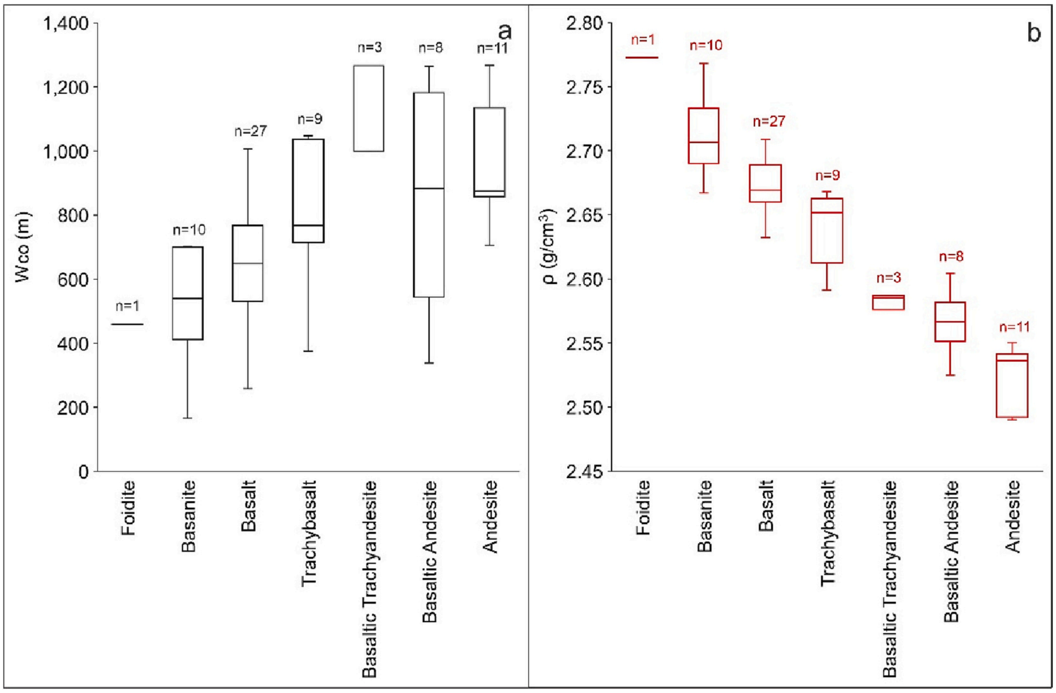

Fig. 7. Boxplots of the relationship between rock type and Wco (a), and between rock type and magma density (b). Wco = Cone base width.

many clusters overlap with the overall average size for a field, there are instances, e.g., Armenia, where they appear to be multi-modal in cone size distributions.

Vent alignments were obtained by two different methods and corresponding references (Table 6). Every alignment is jointly determined by at least two methods, except for alignments in Longgang. The results of the alignment analysis in Longgang are not obvious (Supplementary Fig. 2). However, there are three potential vent alignments (NE-SW, NW-SE and E-W) from the Cebriá et al. (2011) method, which is considered to be consistent with the alignments inferred by Zhao et al. (2021).

Considering cone volumes in relation to vent alignments, it is apparent that volcanoes occurring on fault-controlled alignments tend to have larger Wco (Table 6). Vent alignments that occur approximately parallel with the main tectonic structures of the volcanic fields show the largest average Wco (e.g., Armenia, Chichinautzin, Jeju Island, Todra; Table 6). Wco seems to be further correlated with the type of fault, in which normal/strike-slip hosts the largest Wco on average compared to reverse faults (e.g., Longgang; Table 6). On the other hand, the long axes of the volcanic field ellipses have little effect on Wco, unless their orientations coincide with the faults where the largest average Wco occurred (Table 6). Furthermore, the distribution of Wco for most single alignments is relatively narrow (see Supplementary Data 4). For example, in Todra, the Wco standard deviation (241 m) of the five vents (dark blue-purple colour) on the NE-SW alignment in cluster 14 is about half the overall standard deviation (457 m) for the field (see Supplementary Data 4).

4. Discussion

4.1. Estimation of lava flow volumes from cone morphometry

The quality and availability of DEMs (e.g., LiDAR, SAR-based DEM, such as WorldDEM) have improved over the years. Those DEM sources have also increasingly been used for the estimation of the volume of volcanic lava flows (Lu et al., 2003; Kereszturi et al., 2013, 2016). This study used available 10 m DEM (NED) in the United States and globally free 30 m DEM (AW3D30) in other regions. NED is a more accurate DEM than AW3D30 (Gesch et al., 2014; Tadono et al., 2016), although only a few studies have explored its use in monogenetic volcanic geomorphology (e.g., Fornaciai et al., 2012). An accuracy evaluation of AW3D30 for scoria cones and associated lava flows shows that the average volume and height errors of scoria cones $\geq 5 \times 10^6$ m^3 are within 4.5% and 8.3%, respectively, and for their associated lava flow $\geq 10 \times 10^6$ m^3, the average volume error does not exceed 11.2% (Zhang et al., 2022). The accuracy of Wco and Wcr increases for better-preserved and less-eroded scoria cones. For instance, the gradual outflow of lava may collapse the flank of scoria cones (e.g., Romero et al., 2022) and consequently increase Wco. Here we found that the geomorphological parameters of better-preserved scoria cones have a good correlation with the volume of their lava flows, and hence parameters like Wco can be used to approximate lava flow volumes if direct measurements are otherwise not possible (e.g., overlapping and burial of flows).

The relationship between intact scoria cone morphometric parameters and Vla (Fig. 4) established in this study is inherently different from Wood (1980) and Porter (1972), due to the parameterization method and the use of DEMs. However, Wood's relationship between Vco and Vla generally mimics our result for Wco when assuming Hco/Wco = 0.18 and Wcr/Wco = 0.40 (Fig. 9). The relationships between Vco and Hco with Vla (red and blue line in Fig. 9, respectively) are noticeably different from that of Wood (1980), which may be due to larger scoria cone population used and the methods to calculate Vco and Hco. This study suggests that the relationship between Vco and Vla related to Wco should be more accurate up to a Vco $\leq 200 \times 10^6$ m^3 (black line in Fig. 9).

4.2. Factors influencing monogenetic volcano volume

Based on the morphometric analysis, tectonic setting and crustal thickness appear to exert a control on the volumes of monogenetic volcanoes. Subduction systems can efficiently generate magma, and the thick crustal structure can further promote magma accumulation and mid- to upper-crustal storage (Tatsumi, 1989; Farner and Lee, 2017; Paguican et al., 2021). By comparing the output rates of volcanic fields (e.g., volume per area), the degree of magma supply can be understood.

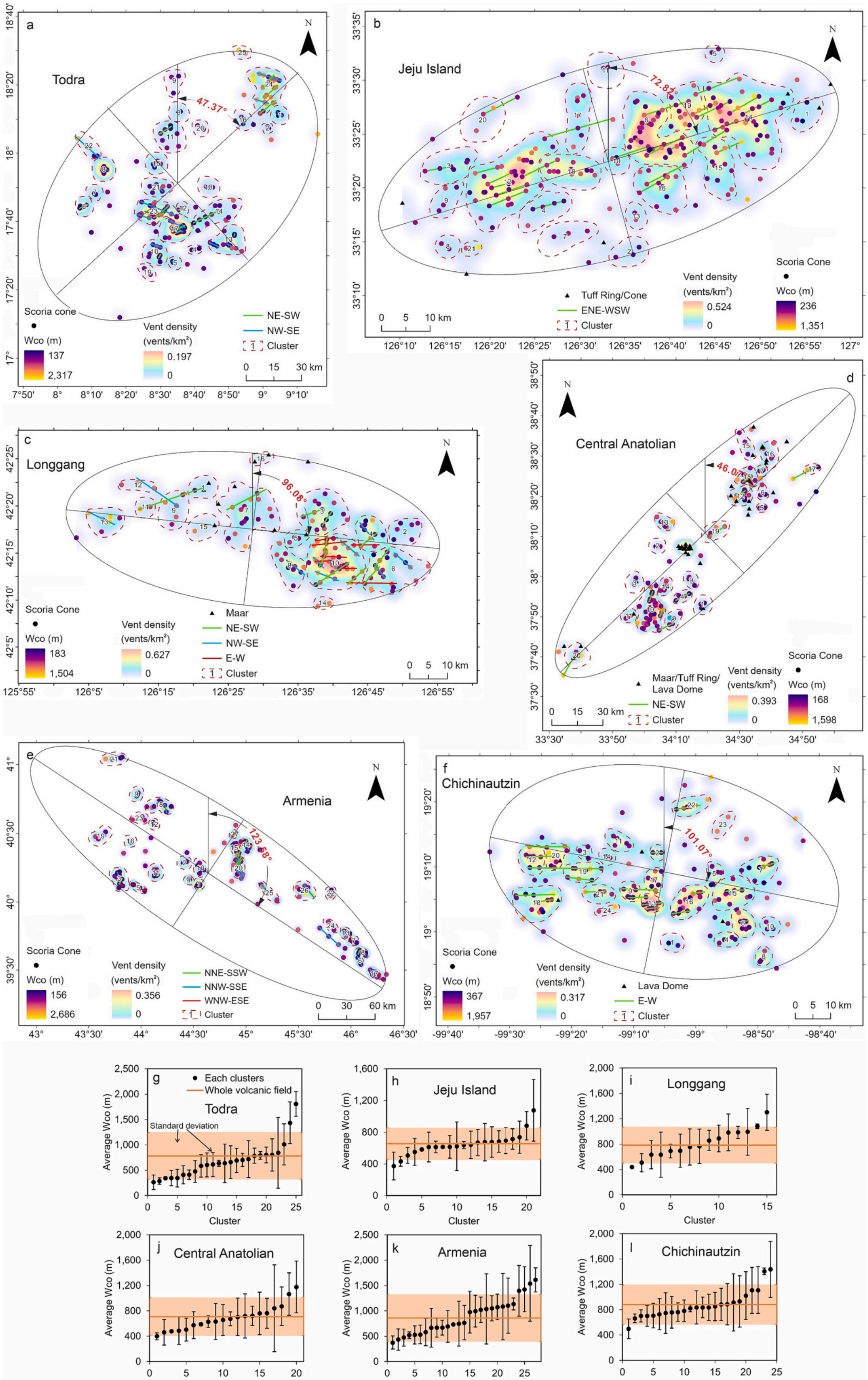

Fig. 8. (a–f) Minimum ellipse, scoria cone volume distribution, vent cluster and alignment of selected volcanic fields. Ellipses mark the calculated minimum ellipses of each volcanic field. Red numbers indicate the angles of the long axes of the ellipses. Vent alignments of each volcanic field are summarized by the methods of Lutz (1986) and Cebriá et al. (2011) as well as previous studies (e.g., Le Corvec et al., 2013; Zhao et al., 2021). (g–l) Comparison of the average Wco of individual clusters and the overall average Wco of each volcanic field. Wco = Cone base width.

Table 6
Vent alignment and Wco distribution results of selected six volcanic fields.

Volcanic field	Long axis azimuth of ellipse	Fault			Vent alignment		Number of cones	Wco (m)	
		Direction	Type	Reference	Reference	Alignment		Mean	Std
Armenia	124°	NNW-SSE	Strike-Slip	Philip et al., 2001		Whole	218	858	462
					Cebriá et al., 2011; Le Corvec et al., 2013	NNE-SSW	31	711	362
					Cebriá et al., 2011; Le Corvec et al., 2013	**NNW-SSE**	**56**	**986**	**517**
					Lutz, 1986; Cebriá et al., 2011	WNW-ESE	32	715	345
						Others	116	872	462
Central Anatolian	46°	NW-SE	Normal	Gürsoy et al., 1998	Lutz, 1986; Cebriá et al., 2011	Whole	136	711	298
		NE-SW	Normal			**NE-SW**	**38**	**742**	**326**
						Others	98	700	287
Chichinautzin	101°	E-W	Normal	Arce et al., 2015		whole	171	878	311
					Lutz, 1986; Cebriá et al., 2011; Le Corvec et al., 2013	**E-W**	**64**	**901**	**307**
						Others	107	864	313
Jeju Island	73°	ENE-WSW	Normal	Brenna et al., 2015		whole	220	655	198
					Lutz, 1986; Le Corvec et al., 2013	**ENE-WSW**	**83**	**694**	**183**
						Others	137	631	203
Longgang	96°	NE-SW	Strike-Slip	Zhao et al., 2021		whole	140	781	281
		NW-SE	Strike-Slip		Zhao et al., 2021	NE-SW	35	806	225
		E-W	Reverse		Zhao et al., 2021	**NW-SE**	**31**	**909**	**271**
					Zhao et al., 2021	E-W	21	884	193
						Others	69	699	292
Todra	47°	NW-SE	Normal	Liégeois et al., 2005		whole	188	781	457
					Lutz, 1986; Le Corvec et al., 2013	NE-SW	60	702	392
					Lutz, 1986; Cebriá et al., 2011; Le Corvec et al., 2013	**NW-SE**	**46**	**833**	**482**
						Others	87	785	462

Wco = Cone base width.
Note that bold font represents the vent alignment where the largest average Wco occurs in each volcanic field.

However, assessing the eruption volume of a volcanic field is cumbersome and requires the integration of multiple data, such as drilling data (Brenna et al., 2015), which makes the output rate available for each volcanic field very limited. In some volcanic fields, scoria cones account for the majority of volcano types (Table 7). This study found that Wco or Aco is an index parameter that can represent the total volume of an individual scoria cone and associated lava flow. Therefore, we can evaluate the planimetric scoria cone output rate by calculating the total area of all scoria cones in a volcanic field over the lifespan of the field. However, it should be noted that this approach does not account for the volumes of tephra blanket, and other edifices, such as maars, tuff rings, and lava domes (Table 7). There is a particularly good correlation between planimetric scoria cone output rates and volumetric volcanic output rates (Fig. 10). In general, the output rate of subduction volcanic fields is considerably larger than that of intraplate volcanic fields. For example, the planimetric scoria cone output rate and the volumetric volcanic output rate of the Chichinautzin Volcanic Field are 2.91 km^2/kyr and 11.75 km^3/kyr, respectively, while those of the Southwestern Nevada Volcanic Field are 0.003 km^2/kyr and 0.0005 km^3/kyr, respectively. This suggests that in subduction environments average magma generation and output rates enable the formation and growth of larger monogenetic cones. Furthermore, crustal settings (e.g., thicker crust) can also effectively influence Wco (Schmidt et al., 2022), hence positively reinforcing this observation.

The physical and chemical properties of magma are important factors in controlling the volume of monogenetic volcanoes, affecting the ascent of magma from source to surface. In the Philippines, Paguican et al. (2021) found that larger volcanoes tend to have more silicic compositions, which is consistent with our results. The chemical properties of magma largely determine its physical properties. Magma density can strongly control lava volume, while magma viscosity has a lesser effect (Hartley and Maclennan, 2018). Thus, under the same environment and overpressure, magma with lower density and viscosity has a greater flux rate to facilitate the eruption, once a volcanic vent is opened (i.e., tectonically favorable conditions). Likewise, for monogenetic volcanic cones, we found that density has an inverse relationship with Wco (Fig. 6j), indicating that lower density magmas form larger cones. This may be related not only to greater magma buoyancy but also to more exsolved gases (Wallace et al., 2015). The exsolved gases can accelerate the rising of the magma and generate explosive volcanoes so that the volume of the volcano becomes larger (Parfitt, 2004). When magma and its bubbles are effectively decoupled during ascent the magma is outgassed resulting in effusive-like eruption with mild lava fountaining (Parfitt, 2004), building up volcanic edifices with small Wco and Hco. Furthermore, such edifices are often dominated by welding and agglutination depending on the fragment ejection rate (Head and Wilson, 1989), resulting in a pyroclastic succession dominated by vesicle-poor deposits. At another extreme, cones formed from violent Strombolian eruptions from frothy magma (Pioli et al., 2009) lead to larger edifices.

Our study shows that pre-existing fault systems are also important factors controlling Wco. While the melt can homogeneously be generated at the source, it comes to the surface along pre-existing faults hence facilitating larger monogenetic eruptions (Valentine and Krogh, 2006) with influences from local stress variations (Martí et al., 2016). In an extensional or strike-slip environment, the maximum or the intermediate principal stress is vertical, and dikes tend to propagate vertically, meaning that magma is more likely to be emplaced to the surface, whereas in a compressional environment, the least principal stress is vertical and sills are common (Haag et al., 2019). This is illustrated in Longgang Volcanic Field, where the larger volume cones are distributed along NW-SE strike-slip fault sets that are approximately perpendicular to the overall EW-dominated compressional stress regime (Table 6). In

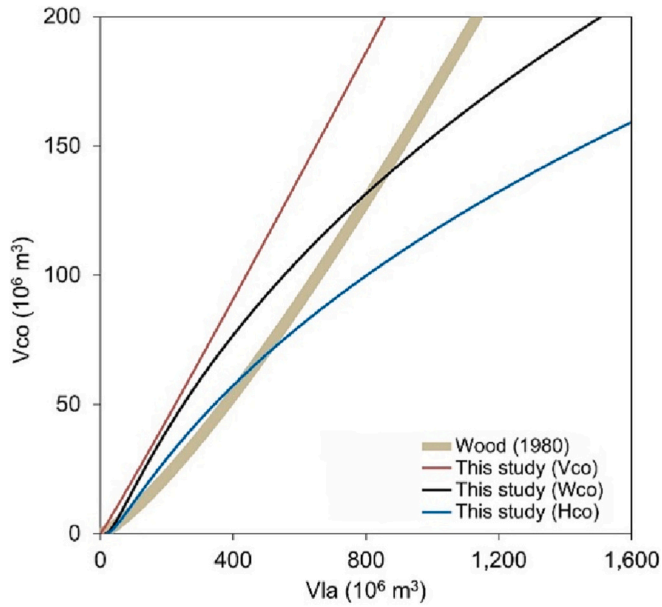

Fig. 9. Comparison of different volume relationships between scoria cones and associated lava flows. Vco derived from Wco and Hco, respectively, is calculated according to eq. (2) of Riedel et al. (2003), which assumes cones have reached the angle of repose and Hco/Wco and Wcr/Wco are the ideal values proposed by Porter (1972) and Wood (1980). Vla derived from Wco and Hco is based on Eq. 7 and Eq. 8, respectively. The red line is the relationship between Vco and Vla for the intact cones in Fig. 4d. Vco = Cone volume, Vla = Lava flow volume, Hco = Cone height, and Wco = Cone base width. (For interpretation of the references to colour in this figure legend, the reader is referred to the web version of this article.)

compressional environments, although pre-existing crustal structures can still assist magma ascent to the surface (Galland et al., 2003), these environments typically host smaller monogenetic volcanoes. On the other hand, the shape of the volcanic field has no significant effect on the volume of individual volcanoes, possibly because they may be controlled not only by the tectonic environment but also by magma-generation processes (Le Corvec et al., 2013; Runge et al., 2015), which may have little significance for volume output variations at a local scale.

Factors affecting the volumes of monogenetic volcanoes should be considered holistically, because both regional and local tectonic settings can be interlinked with the generation and migration of magma. For example, mostly, the local environment tends to be compressional near the subduction trench with larger and more differentiated magma supply. Hence these conditions are favorable for generating larger volume volcanic eruptions, coined before as “magmatically controlled” volcanic fields which are characterized by relatively high magma fluxes (Valentine and Perry, 2007). In such setting, the magmatic overpressure may predominate compared to local stress patterns, and therefore, the occurrence of larger volcanoes becomes random within the field, although naturally magma availability and evolution can influence this (e.g., Villamor et al., 2017). Conversely, intraplate and rift settings are more “tectonically controlled” (Valentine and Perry, 2007), and our results show that larger volume volcanoes can appear along pre-existing fault systems associated with extensional or strike-slip local stresses (Table 6). This implies that the relationship between fracture distribution and volcanic volume should be implicitly included in volcanic hazard assessment of distributed monogenetic fields in intraplate and rift environments.

4.3. Limitations

The delineation of Aco and Acr has been carried out manually, and therefore their accuracy cannot be objectively quantified. Semi-automatic methods of edifice delineation can be used to improve objectivity (Bohnenstiehl et al., 2012; Euillades et al., 2013), although those approaches only take into consideration the morphology without lithological information. However, we combined multi-source data, including optical satellite imagery, topographic and elevation data for

Table 7
Comparison of output rate in different volcanic fields.

Volcanic field	Number of volcanoes	% of scoria cones	Cumulative scoria cone area (km^2)	Cumulative volume (km^3)	Duration of output (kyr)	Planimetric scoria cone output rate (km^2/kyr)	Volumetric volcanic output rate (km^3/kyr)	Reference
Antofagasta de la Sierra	58	100%	32.246	21.272[a]	**7000**	0.005	0.003	Báez et al., 2017
Auckland	**52**	**73%**	**7.461**	**3.135**	**250**	**0.030**	**0.013**	Kereszturi et al., 2013
Central Anatolian	170	80%	63.485	24.739[a]	**3200**	0.020	0.008	Gürsoy et al., 1998
Chichinautzin	175	98%	116.408	**470**	**40**	2.910	**11.75**	Arce et al., 2015; Márquez et al., 1999
Colima	11	100%	10.056	**1.4**	**1200**	0.008	**0.001**	Carmichael et al., 2006
Jeju Island	227	97%	80.811	**568**	**1700**	0.048	**0.334**	Brenna et al., 2015
Longgang	150	93%	75.005	27.129[a]	**2150**	0.035	0.013	Fan et al., 2002
Michoacán-Guanajuato	1031	92%	541.819	1626[b]	**3000**	0.181	0.542	Hasenaka, 1994
Newer	238	83%	134.571	91.389[a]	**1290**	0.104	0.071	Oostingh et al., 2017
Payenia	933	98%	296.485	111.947[a]	**2000**	0.148	0.056	May et al., 2018
San Francisco	460	95%	327.628	**510**	**5000**	0.066	**0.102**	Tanaka et al., 1986
Southwestern Nevada	36	100%	8.524	**0.575**	**2900**	0.003	**0.0005**	Valentine and Perry, 2007
Springerville	407	97%	171.210	**300**	**1800**	0.095	**0.167**	Condit et al., 1989
Wudalianchi	23	100%	8.036	2.718[a]	**4600**	0.002	0.0006	Zhao et al., 2014

Note that bold font represents data cited from references.
[a] Volume is the total volume of scoria cones and associated lava flows calculated from Wco. Vco is calculated according to eq. (2) of Riedel et al. (2003), which assumes cones have reached the angle of repose and Hco/Wco and Wcr/Wco are the ideal values proposed by Porter (1972) and Wood (1980). Vla is based on Eq. 5.
[b] Minimum bulk volume was estimated from dense rock equivalent volume divided by 0.7 (Hasenaka, 1994).

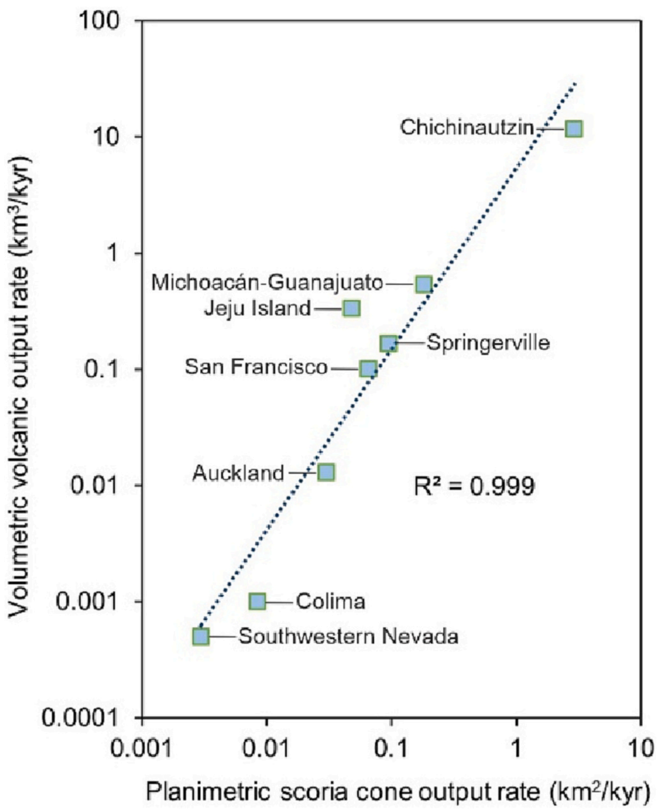

Fig. 10. Comparison between planimetric scoria cone output rate and volumetric volcanic output rate. Note the log-log scale. The blue dash line is a power trend line. (For interpretation of the references to colour in this figure legend, the reader is referred to the web version of this article.)

objective delineation of the cones and flows.

Due to the accuracy limitations of the AW3D30 data, the relationship of Vco and Hco to Vla was not considered when scoria cone volumes were $\leq 5 \times 10^6$ m^3 and/or associated lava flow volumes were $\leq 10 \times 10^6$ m^3. However, there were ten scoria cones with volumes $<5 \times 10^6$ m^3, but their associated lava flow volumes all exceeded 10×10^6 m^3 (Table 3). Therefore, the relationship of Wco and Wcr to Vla for these scoria cones is relatively reliable. Higher resolution data (e.g., WorldDEM or LiDAR) are necessary to refine the volumetric relationship for small-volume edifices.

No volume assessments have been made for the distal tephra deposits of monogenetic volcanoes, although they represent only a small fraction of the total volume (e.g., Kereszturi et al., 2013). Other monogenetic volcanic edifices, such as maars, tuff rings, tuff cones, and lava domes were also not considered, although, depending on environmental factors, they may make up only a small proportion of vents in a volcanic field (Table 7).

5. Conclusions

Our study has confirmed the complex relationship between scoria cone geomorphological parameters and the volume of their associated lava flows, based on globally available, free-to-access AW3D30 DEM and the country-wide NED DEM in the USA, as well as various satellite images and terrain maps. It is concluded that Wco is the best morphometric parameter to indicate the volume of lava flows related to individual scoria cones. When the proportion of scoria cones among the total number of vents in a volcanic field exceeds 90%, the planimetric scoria cone output rate is a reliable parameter for evaluating the magma flux rate.

Regional tectonic factors, such as tectonic setting and crust thickness, are key to controlling the volume of eruptible monogenetic magma. Subduction settings and crust thickness > 35 km are associated with larger monogenetic volcanoes because these regional tectonic factors are likely related to the larger amount of magma generated and/or stalled. Pre-existing fault systems also facilitate magma migration in the upper crust. The largest average-sized scoria cones are generally situated along fault systems and are influenced by local stresses, with a lesser impact from magma source shapes.

The chemical and physical properties of magma are also important controls affecting the amount of eruptible magma. The melt density strongly controls the resulting eruptive volumes, with the two being inversely proportional, suggesting that increased magma flux rates in volcanic plumbing systems are associated with decreased melt density.

CRediT authorship contribution statement

Rong Zhang: Conceptualization, Methodology, Formal analysis, Resources, Writing – original draft, Visualization. **Marco Brenna:** Methodology, Resources, Writing – review & editing, Supervision. **Gabor Kereszturi:** Methodology, Resources, Writing – review & editing.

Declaration of Competing Interest

The authors declare that they have no known competing financial interests or personal relationships that could have appeared to influence the work reported in this paper.

Data availability

Data will be made available on request.

Acknowledgements

We thank the Pūtea Tautoko - Student Relief Fund and the Doctoral Postgraduate Publishing Bursary provided by the University of Otago. We gratefully acknowledge Martha Gabriela Gómez-Vasconcelos and an anonymous reviewer for their insightful comments and suggestions to improve the manuscript.

Appendix A. Supplementary data

Supplementary data to this article can be found online at https://doi.org/10.1016/j.jvolgeores.2023.107872.

References

Agustín-Flores, J., Siebe, C., Guilbaud, M.N., 2011. Geology and geochemistry of Pelagatos, Cerro del Agua, and Dos Cerros monogenetic volcanoes in the Sierra Chichinautzin volcanic field, south of Mexico City. J. Volcanol. Geotherm. Res. 201 (1–4), 143–162. https://doi.org/10.1016/j.jvolgeores.2010.08.010.

Ahmed, A., Tiberi, C., Leroy, S., Stuart, G.W., Keir, D., Sholan, J., Khanbari, K., Al-Ganad, I., Basuyau, C., 2013. Crustal structure of the rifted volcanic margins and uplifted plateau of Western Yemen from receiver function analysis. Geophys. J. Int. 193 (3), 1673–1690. https://doi.org/10.1093/gji/ggt072.

Ahmed, A.H., Moghazi, A.K.M., Moufti, M.R., Dawood, Y.H., Ali, K.A., 2016. Nature of the lithospheric mantle beneath the Arabian Shield and genesis of Al-spinel micropods: evidence from the mantle xenoliths of Harrat Kishb, Western Saudi Arabia. Lithos 240, 119–139. https://doi.org/10.1016/j.lithos.2015.11.016.

Aldrich Jr., M.J., Laughlin, A.W., 1984. A model for the tectonic development of the southeastern Colorado Plateau boundary. J. Geophys. Res. Solid Earth 89 (B12), 10207–10218. https://doi.org/10.1029/JB089iB12p10207.

Al-Fakih, R., Li, K., 2018. Study of geothermal energy resources of Yemen for electric power generation. Trans. Geotherm. Resour. Counc. 42, 777–795.

Alıcı, P., Temel, A., Gourgaud, A., 2002. Pb–Nd–Sr isotope and trace element geochemistry of Quaternary extension-related alkaline volcanism: a case study of Kula region (western Anatolia, Turkey). J. Volcanol. Geotherm. Res. 115 (3–4), 487–510. https://doi.org/10.1016/S0377-0273(01)00328-6.

Aoki, Y., Tsunematsu, K., Yoshimoto, M., 2019. Recent progress of geophysical and geological studies of Mt. Fuji Volcano, Japan. Earth Sci. Rev. 194, 264–282. https://doi.org/10.1016/j.earscirev.2019.05.003.

Arce, J.L., Muñoz-Salinas, E., Castillo, M., Salinas, I., 2015. The~ 2000 yr BP Jumento volcano, one of the youngest edifices of the Chichinautzin Volcanic Field, Central

Mexico. J. Volcanol. Geotherm. Res. 308, 30–38. https://doi.org/10.1016/j.jvolgeores.2015.10.008.
Badri, M., 1991. Crustal structure of Central Saudi Arabia determined from seismic refraction profiling. Tectonophysics 185 (3–4), 357–374. https://doi.org/10.1016/0040-1951(91)90454-Z.
Báez, W., Bustos, E., Chiodi, A., Reckziegel, F., Arnosio, M., de Silva, S., Giordano, G., Viramonte, J.G., Sampietro-Vattuone, M.M., Peña-Monné, J.L., 2020. Eruptive style and flow dynamics of the pyroclastic density currents related to the Holocene Cerro Blanco eruption (Southern Puna plateau, Argentina). J. S. Am. Earth Sci. 98, 102482. https://doi.org/10.1016/j.jsames.2019.102482.
Báez, W., Carrasco Nuñez, G., Giordano, G., Viramonte, J.G., Chiodi, A., 2017. Polycyclic scoria cones of the Antofagasta de la Sierra basin, Southern Puna plateau, Argentina. Geol. Soc. Lond. Spec. Publ. 446, 311–336. https://doi.org/10.1144/SP446.3.
Bahri, S., Suryanto, W., Ngadmanto, D., 2021. Sediment thickness and moho depth beneath western Indonesian region from teleseismic receiver function. Res. Square. https://doi.org/10.21203/rs.3.rs-356661/v1.
Bohnenstiehl, D.R., Howell, J.K., White, S.M., Hey, R.N., 2012. A modified basal outlining algorithm for identifying topographic highs from gridded elevation data, part 1: motivation and methods. Comput. Geosci. 49, 308–314. https://doi.org/10.1016/j.cageo.2012.04.023.
Brenna, M., Cronin, S.J., Smith, I.E., Sohn, Y.K., Németh, K., 2010. Mechanisms driving polymagmatic activity at a monogenetic volcano, Udo, Jeju Island, South Korea. Contrib. Mineral. Petrol. 160 (6), 931–950. https://doi.org/10.1007/s00410-010-0515-1.
Brenna, M., Cronin, S.J., Nemeth, K., Smith, I.E., Sohn, Y.K., 2011. The influence of magma plumbing complexity on monogenetic eruptions, Jeju Island, Korea. Terra Nova 23 (2), 70–75. https://doi.org/10.1111/j.1365-3121.2010.00985.x.
Brenna, M., Cronin, S.J., Kereszturi, G., Sohn, Y.K., Smith, I.E., Wijbrans, J., 2015. Intraplate volcanism influenced by distal subduction tectonics at Jeju Island, Republic of Korea. Bull. Volcanol. 77 (1), 1–16. https://doi.org/10.1007/s00445-014-0896-5.
Brenna, M., Cronin, S.J., Smith, I.E., Tollan, P.M., Scott, J.M., Prior, D.J., Bambery, K., Ukstins, I.A., 2018. Olivine xenocryst diffusion reveals rapid monogenetic basaltic magma ascent following complex storage at Pupuke Maar, Auckland Volcanic Field, New Zealand. Earth Planet. Sci. Lett. 499, 13–22. https://doi.org/10.1016/j.epsl.2018.07.015.
Brenna, M., Ubide, T., Nichols, A.R., Mollo, S., Pontesilli, A., 2021. Anatomy of intraplate monogenetic alkaline basaltic magmatism: clues from magma, crystals, and glass. In: Crustal Magmatic System Evolution: Anatomy, Architecture, and Physico-Chemical Processes, pp. 79–103. https://doi.org/10.1002/9781119564485.ch4.
Camp, V.E., Roobol, M.J., Hooper, P.R., 1992. The Arabian continental alkali basalt province: Part III. Evolution of Harrat Kishb, Kingdom of Saudi Arabia. Geol. Soc. Am. Bull. 104 (4), 379–396. https://doi.org/10.1130/0016-7606(1992)104<0379:TACABP>2.3.CO;2.
Carmichael, I.S.E., Frey, H.M., Lange, R.A., Hall, C.M., 2006. The Pleistocene cinder cones surrounding Volcán Colima, Mexico re-visited: eruption ages and volumes, oxidation states, and sulfur content. Bull. Volcanol. 68 (5), 407–419. https://doi.org/10.1007/s00445-005-0015-8.
Carn, S.A., 2000. The Lamongan volcanic field, East Java, Indonesia: physical volcanology, historic activity and hazards. J. Volcanol. Geotherm. Res. 95 (1–4), 81–108. https://doi.org/10.1016/S0377-0273(99)00114-6.
Carn, S.A., Pyle, D.M., 2001. Petrology and geochemistry of the Lamongan volcanic field, East Java, Indonesia: Primitive Sunda arc magmas in an extensional tectonic setting? J. Petrol. 42 (9), 1643–1683. https://doi.org/10.1093/petrology/42.9.1643.
Carracedo, J.C., Badiola, E.R., Guillou, H., Paterne, M., Scaillet, S., Torrado, F.P., Paris, R., Fra-Paleo, U., Hansen, A., 2007. Eruptive and structural history of Teide Volcano and rift zones of Tenerife, Canary Islands. Geol. Soc. Am. Bull. 119 (9–10), 1027–1051. https://doi.org/10.1130/B26087.1.
Cebriá, J.M., Martín-Escorza, C., López-Ruiz, J., Morán-Zenteno, D.J., Martiny, B.M., 2011. Numerical recognition of alignments in monogenetic volcanic areas: examples from the Michoacán-Guanajuato Volcanic Field in Mexico and Calatrava in Spain. J. Volcanol. Geotherm. Res. 201 (1–4), 73–82. https://doi.org/10.1016/j.jvolgeores.2010.07.016.
Chernet, T., 2011. Geology and hydrothermal resources in the northern Lake Abaya area (Ethiopia). J. Afr. Earth Sci. 61 (2), 129–141. https://doi.org/10.1016/j.jafrearsci.2011.05.006.
Condit, C.D., Crumpler, L.S., Aubele, J.C., Elston, W.E., 1989. Patterns of volcanism along the southern margin of the Colorado Plateau: the Springerville field. J. Geophys. Res. Solid Earth 94 (B6), 7975–7986. https://doi.org/10.1029/JB094iB06p07975.
Connor, C.B., 1990. Cinder cone clustering in the TransMexican Volcanic Belt: implications for structural and petrologic models. J. Geophys. Res. Solid Earth 95 (B12), 19395–19405. https://doi.org/10.1029/JB095iB12p19395.
Connor, C.B., Conway, F.M., 2000. Basaltic volcanic fields. In: Sigurdsson, H. (Ed.), Encyclopedia of Volcanoes. Academic Press, San Diego, pp. 331–343.
Danyushevsky, L.V., Plechov, P., 2011. Petrolog3: Integrated software for modeling crystallization processes. Geochem. Geophys. Geosyst. 12 (7) https://doi.org/10.1029/2011GC003516.
Davis, J.C., 2002. Statistics and Data Analysis in Geology, 3rd Ed. John Wiley & Sons.
Day, S.J., Carracedo, J.C., Guillou, H., Gravestock, P., 1999. Recent structural evolution of the Cumbre Vieja volcano, La Palma, Canary Islands: volcanic rift zone reconfiguration as a precursor to volcano flank instability? J. Volcanol. Geotherm. Res. 94 (1–4), 135–167. https://doi.org/10.1016/S0377-0273(99)00101-8.
De Fino, M., La Volpe, L., Lirer, L., 1973. Volcanology and petrology of the Assab range (Ethiopia). Bull. Volcanol. 37 (1), 95–110. https://doi.org/10.1007/BF02596882.
Di Roberto, A., Risica, G., Del Carlo, P., Pompilio, M., Speranza, F., Meletlidis, S., 2020. The forgotten eruption: the basaltic scoria cone of Montaña Grande, Tenerife. J. Volcanol. Geotherm. Res. 401, 106918 https://doi.org/10.1016/j.jvolgeores.2020.106918.
Dirksen, O.V., Bazanova, L.I., 2010. An eruption of the veer cone as a volcanic event during the increase of volcanic activity in Kamchatka at the beginning of the Christian Era. J. Volcanol. Seismol. 4 (6), 378–384. https://doi.org/10.1134/S0742046310060023.
Downs, D.T., Robinson, J.E., Stelten, M.E., Champion, D.E., Dieterrich, H.R., Sisson, T. W., Zahran, H., Hassan, K., Shawali, J., 2019. Geologic map of the northern Harrat Rahat volcanic field. Kingdom of Saudi Arabia. US Geological Survey Scientific Investigations Map 3428. https://doi.org/10.3133/sim3428.
Duan, Y.H., Zhang, X.K., Liu, Z., Yuan, Q.X., Xu, Z.F., Wang, F.Y., Fang, S.M., Yang, Z.X., 2005. Study on crustal structures of Changbaishan-Jingpohu volcanic area using receiver functions. Chin. J. Geophys. 48 (2), 389–396. https://doi.org/10.1002/cjg2.665.
Dugda, M.T., Nyblade, A.A., Julia, J., Langston, C.A., Ammon, C.J., Simiyu, S., 2005. Crustal structure in Ethiopia and Kenya from receiver function analysis: implications for rift development in eastern Africa. J. Geophys. Res. Solid Earth 110 (B1). https://doi.org/10.1029/2004JB003065.
Duncan, R.A., Al-Amri, A.M., 2013. Timing and composition of volcanic activity at Harrat Lunayyir, western Saudi Arabia. J. Volcanol. Geotherm. Res. 260, 103–116. https://doi.org/10.1016/j.jvolgeores.2013.05.006.
El Tahir, N., Nyblade, A., Julià, J., Durrheim, R., 2013. Crustal structure of the Khartoum Basin, Sudan. Tectonophysics 593, 151–160. https://doi.org/10.1016/j.tecto.2013.02.032.
Erlund, E.J., Cashman, K.V., Wallace, P.J., Pioli, L., Rosi, M., Johnson, E., Granados, H. D., 2010. Compositional evolution of magma from Parícutin Volcano, Mexico: the tephra record. J. Volcanol. Geotherm. Res. 197 (1–4), 167–187. https://doi.org/10.1016/j.jvolgeores.2009.09.015.
Euillades, L.D., Grosse, P., Euillades, P.A., 2013. NETVOLC: an algorithm for automatic delimitation of volcano edifice boundaries using DEMs. Comput. Geosci. 56, 151–160. https://doi.org/10.1016/j.cageo.2013.03.011.
Fan, Q.C., Sui, J.L., Liu, R.X., Wei, H.Q., Li, D.M., Sun, Q., Li, N., 2002. Periods of Quaternary volcanic activity in Longgang area, Jilin province. Acta Petrol. Sin. 18 (4), 495–500 (in Chinese).
Farner, M.J., Lee, C.T.A., 2017. Effects of crustal thickness on magmatic differentiation in subduction zone volcanism: a global study. Earth Planet. Sci. Lett. 470, 96–107. https://doi.org/10.1016/j.epsl.2017.04.025.
Favalli, M., Karátson, D., Mazzarini, F., Pareschi, M.T., Boschi, E., 2009. Morphometry of scoria cones located on a volcano flank: a case study from Mt. Etna (Italy), based on high-resolution LiDAR data. J. Volcanol. Geotherm. Res. 186 (3–4), 320–330. https://doi.org/10.1016/j.jvolgeores.2009.07.011.
Fenton, C.R., Niedermann, S., 2014. Surface exposure dating of young basalts (1–200 ka) in the San Francisco volcanic field (Arizona, USA) using cosmogenic 3He and 21Ne. Quat. Geochronol. 19, 87–105. https://doi.org/10.1016/j.quageo.2012.10.003.
Fornaciai, A., Favalli, M., Karátson, D., Tarquini, S., Boschi, E., 2012. Morphometry of scoria cones, and their relation to geodynamic setting: a DEM-based analysis. J. Volcanol. Geotherm. Res. 217, 56–72. https://doi.org/10.1016/j.jvolgeores.2011.12.012.
Franz, G., Breitkreuz, C., Coyle, D.A., El Hur, B., Heinrich, W., Paulick, H., Pudlo, D., Smith, R., Steiner, G., 1997. The alkaline Meidob volcanic field (late Cenozoic, northwest Sudan). J. Afr. Earth Sci. 25 (2), 263–291. https://doi.org/10.1016/S0899-5362(97)00103-6.
Galland, O., De Bremond d'Ars, J., Cobbold, P.R., Hallot, E., 2003. Physical models of magmatic intrusion during thrusting. Terra Nova 15 (6), 405–409. https://doi.org/10.1046/j.1365-3121.2003.00512.x.
Gesch, D.B., Oimoen, M.J., Evans, G.A., 2014. Accuracy assessment of the US geological survey national elevation dataset, and comparison with other large-area elevation datasets: SRTM and ASTER. In: U.S. Geological Survey Open-File Report 2014-1008, p. 10. https://doi.org/10.3133/ofr20141008.
Gesch, D.B., Evans, G.A., Oimoen, M.J., Arundel, S., 2018. The National Elevation Dataset. In: Maune, D.F., Nayegandhi, A. (Eds.), Digital Elevation Model Technologies and Applications: The DEM Users Manual, 3rd ed. American Society for Photogrammetry and Remote Sensing, pp. 83–110.
Gilbert, H., Velasco, A.A., Zandt, G., 2007. Preservation of Proterozoic terrane boundaries within the Colorado Plateau and implications for its tectonic evolution. Earth Planet. Sci. Lett. 258 (1–2), 237–248. https://doi.org/10.1016/j.epsl.2007.03.034.
Giordano, D., Russell, J.K., Dingwell, D.B., 2008. Viscosity of magmatic liquids: a model. Earth Planet. Sci. Lett. 271 (1–4), 123–134. https://doi.org/10.1016/j.epsl.2008.03.038.
González-Maurel, O., Godoy, B., Le Roux, P., Rodríguez, I., Marín, C., Menzies, A., Bertin, D., Morata, D., Vargas, M., 2019. Magmatic differentiation at La Poruña scoria cone, Central Andes, northern Chile: evidence for assimilation during turbulent ascent processes, and genetic links with mafic eruptions at adjacent San Pedro volcano. Lithos 338, 128–140. https://doi.org/10.1016/j.lithos.2019.03.033.
Grosse, P., De Vries, B.V.W., Euillades, P.A., Kervyn, M., Petrinovic, I.A., 2012. Systematic morphometric characterization of volcanic edifices using digital elevation models. Geomorphology 136 (1), 114–131. https://doi.org/10.1016/j.geomorph.2011.06.001.
Guilbaud, M.N., Siebe, C., Layer, P., Salinas, S., 2012. Reconstruction of the volcanic history of the Tacámbaro-Puruarán area (Michoacán, México) reveals high frequency of Holocene monogenetic eruptions. Bull. Volcanol. 74 (5), 1187–1211. https://doi.org/10.1007/s00445-012-0594-0.

Guillou, H., Carracedo, J.C., Day, S.J., 1998. Dating of the upper Pleistocene–Holocene volcanic activity of La Palma using the unspiked K-Ar technique. J. Volcanol. Geotherm. Res. 86 (1–4), 137–149. https://doi.org/10.1016/S0377-0273(98)00074-2.

Guillou, H., Carracedo, J.C., Duncan, R.A., 2001. K-Ar, 40Ar-39Ar ages and magnetostratigraphy of Brunhes and Matuyama lava sequences from La Palma Island. J. Volcanol. Geotherm. Res. 106 (3–4), 175–194. https://doi.org/10.1016/S0377-0273(00)00294-8.

Gürsoy, H., Piper, J.D.A., Tatar, O., Mesci, L., 1998. Palaeomagnetic study of the Karaman and Karapinar volcanic complexes, central Turkey: neotectonic rotation in the south-central sector of the Anatolian Block. Tectonophysics 299 (1–3), 191–211. https://doi.org/10.1016/S0040-1951(98)00205-4.

Haag, M.B., Baez, W.A., Sommer, C.A., Arnosio, J.M., Filipovich, R.E., 2019. Geomorphology and spatial distribution of monogenetic volcanoes in the southern Puna Plateau (NW Argentina). Geomorphology 342, 196–209. https://doi.org/10.1016/j.geomorph.2019.06.008.

Hammer, J.E., Coombs, M.L., Shamberger, P.J., Kimura, J.I., 2006. Submarine sliver in North Kona: a window into the early magmatic and growth history of Hualalai Volcano, Hawaii. J. Volcanol. Geotherm. Res. 151 (1–3), 157–188. https://doi.org/10.1016/j.jvolgeores.2005.07.028.

Hartley, M., Maclennan, J., 2018. Magmatic densities control erupted volumes in Icelandic volcanic systems. Front. Earth Sci. 6, 29. https://doi.org/10.3389/feart.2018.00029.

Hasenaka, T., 1994. Size, distribution, and magma output rate for shield volcanoes of the Michoacán-Guanajuato volcanic field, Central Mexico. J. Volcanol. Geotherm. Res. 63 (1–2), 13–31. https://doi.org/10.1016/0377-0273(94)90016-7.

Hasenaka, T., Carmichael, I.S.E., 1985. A compilation of location, size, and geomorphological parameters of volcanoes of the Michoacan-Guanajuato volcanic field, central Mexico. Geofis. Int. 24 (4), 577–607.

Head, J.W., Wilson, L., 1989. Basaltic pyroclastic eruptions: influence of gas-release patterns and volume fluxes on fountain structure, and the formation of cinder cones, spatter cones, rootless flows, lava ponds and lava flows. J. Volcanol. Geotherm. Res. 37 (3–4), 261–271. https://doi.org/10.1016/0377-0273(89)90083-8.

Heineke, C., Niedermann, S., Hetzel, R., Akal, C., 2016. Surface exposure dating of Holocene basalt flows and cinder cones in the Kula volcanic field (Western Turkey) using cosmogenic ^{3}He and ^{10}Be. Quat. Geochronol. 34, 81–91. https://doi.org/10.1016/j.quageo.2016.04.004.

Heizler, M.T., Perry, F.V., Crowe, B.M., Peters, L., Appelt, R., 1999. The age of Lathrop Wells volcanic center: an 40Ar/39Ar dating investigation. J. Geophys. Res. Solid Earth 104 (B1), 767–804. https://doi.org/10.1029/1998JB900002.

HernandeÂz-Pacheco, A., Valls, M.C., 1982. The historic eruptions of La Palma Island (Canarias). Arquipelago: Rev. Univ. Azores: Ser. C Nat. 3, 83–94.

Hill, K.A., Finlayson, D.M., Hill, K.C., Cooper, G.T., 1995. Mesozoic tectonics of the Otway Basin region: the legacy of Gondwana and the active and the active pacific margin-a review and ongoing research. APPEA J. 35, 467–493. https://doi.org/10.1071/AJ94030.

Hughes, R., Collings, A., 2000. Seismic and volcanic hazards affecting the vulnerability of the Sana'a area of Yemen. Geol. Soc. Lond. Spec. Publ. 171 (1), 355–372. https://doi.org/10.1144/GSL.SP.2000.171.01.26.

Iacovino, K., Till, C.B., 2019. DensityX: a program for calculating the densities of magmatic liquids up to 1,627 C and 30 kbar. Volcanica 2 (1), 1–10. https://doi.org/10.30909/vol.02.01.0110.

Ishizuka, Y., Takada, A., Suzuki, Y., Kobayashi, M., Nakano, S., 2007. Eruption ages and whole-rock chemistries of scoria cones on the northern to western slope of Fuji Volcano based on trenching surveys. Bull. Geol. Surv. Jpn. 57, 357–376 (in Japanese).

Karakhanian, A., Djrbashian, R., Trifonov, V., Philip, H., Arakelian, S., Avagian, A., 2002. Holocene-historical volcanism and active faults as natural risk factors for Armenia and adjacent countries. J. Volcanol. Geotherm. Res. 113 (1–2), 319–344. https://doi.org/10.1016/S0377-0273(01)00264-5.

Katsumata, A., 2010. Depth of the Moho discontinuity beneath the Japanese islands estimated by traveltime analysis. J. Geophys. Res. Solid Earth 115 (B4). https://doi.org/10.1029/2008JB005864.

Kereszturi, G., Németh, K., 2012. Monogenetic basaltic volcanoes: Genetic classification, growth, geomorphology and degradation. In: Németh, K. (Ed.), Updates in Volcanology - New Advances in Understanding Volcanic Systems. InTech Open, Rijeka, Croatia, pp. 3–89, 10.5772/51387.10.5772/51387.

Kereszturi, G., Jordan, G., Németh, K., Dóniz-Páez, J.F., 2012. Syn-eruptive morphometric variability of monogenetic scoria cones. Bull. Volcanol. 74 (9), 2171–2185. https://doi.org/10.1007/s00445-012-0658-1.

Kereszturi, G., Németh, K., Cronin, S.J., Agustín-Flores, J., Smith, I.E., Lindsay, J., 2013. A model for calculating eruptive volumes for monogenetic volcanoes-implication for the Quaternary Auckland Volcanic Field, New Zealand. J. Volcanol. Geotherm. Res. 266, 16–33. https://doi.org/10.1016/j.jvolgeores.2013.09.003.

Kereszturi, G., Németh, K., Moufti, M.R., Cappello, A., Murcia, H., Ganci, G., Negro, C.D., Procter, J., Zahran, H.M.A., 2016. Emplacement conditions of the 1256 AD Al-Madinah lava flow field in Harrat Rahat, Kingdom of Saudi Arabia - insights from surface morphology and lava flow simulations. J. Volcanol. Geotherm. Res. 309, 14–30. https://doi.org/10.1016/j.jvolgeores.2015.11.002.

Kervyn, M., Ernst, G.G.J., Carracedo, J.C., Jacobs, P., 2012. Geomorphometric variability of "monogenetic" volcanic cones: evidence from Mauna Kea, Lanzarote and experimental cones. Geomorphology 136 (1), 59–75. https://doi.org/10.1016/j.geomorph.2011.04.009.

Kröchert, J., Buchner, E., 2009. Age distribution of cinder cones within the Bandas del Sur Formation, southern Tenerife, Canary Islands. Geol. Mag. 146 (2), 161–172. https://doi.org/10.1017/S001675680800544X.

Kshirsagar, P., Siebe, C., Guilbaud, M.N., Salinas, S., Layer, P.W., 2015. Late Pleistocene Alberca de Guadalupe maar volcano (Zacapu basin, Michoacán): Stratigraphy, tectonic setting, and paleo-hydrogeological environment. J. Volcanol. Geotherm. Res. 304, 214–236. https://doi.org/10.1016/j.jvolgeores.2015.09.003.

La Femina, P.C., Connor, C.B., Hill, B.E., Strauch, W., Saballos, J.A., 2004. Magma-tectonic interactions in Nicaragua: the 1999 seismic swarm and eruption of Cerro Negro volcano. J. Volcanol. Geotherm. Res. 137 (1–3), 187–199. https://doi.org/10.1016/j.jvolgeores.2004.05.006.

Le Corvec, N., Spörli, K.B., Rowland, J., Lindsay, J., 2013. Spatial distribution and alignments of volcanic centers: clues to the formation of monogenetic volcanic fields. Earth Sci. Rev. 124, 96–114. https://doi.org/10.1016/j.earscirev.2013.05.005.

Lesti, C., Giordano, G., Salvini, F., Cas, R., 2008. Volcano tectonic setting of the intraplate, Pliocene-Holocene, Newer Volcanic Province (southeast Australia): Role of crustal fracture zones. J. Geophys. Res. Solid Earth 113 (B7). https://doi.org/10.1029/2007JB005110.

Levin, V., Park, J., Brandon, M., Lees, J., Peyton, V., Gordeev, E., Ozerov, A., 2002. Crust and upper mantle of Kamchatka from teleseismic receiver functions. Tectonophysics 358 (1–4), 233–265. https://doi.org/10.1016/S0040-1951(02)00426-2.

Liégeois, J., Benhallou, A., Azzouni-Sekkal, A., Yahiaoui, R., Bonin, B., 2005. The Hoggar swell and volcanism: reactivation of the Precambrian Tuareg shield during Alpine convergence and West African Cenozoic volcanism. Special Papers-Geological Society of America 388, 379.

Lin, C.M., Tseng, T.L., Meliksetian, K., Karakhanyan, A., Huang, B.S., Babayan, H., Hu, J. C., Gevorgyan, M., Chang, S.F., Levonyan, A., 2020. Locally thin crust and high crustal VP/VS ratio beneath the Armenian volcanic highland of the Lesser Caucasus: a case for recent delamination. J. Geophys. Res. Solid Earth 125 (9). https://doi.org/10.1029/2019JB019151 e2019JB019151.

Lu, Z., Fielding, E., Patrick, M.R., Trautwein, C.M., 2003. Estimating lava volume by precision combination of multiple baseline spaceborne and airborne interferometric synthetic aperture radar: the 1997 eruption of Okmok volcano, Alaska. Trans. Geosci. Remote Sens. 41 (6), 1428–1436. https://doi.org/10.1109/TGRS.2003.811553.

Lutz, T.M., 1986. An analysis of the orientations of large-scale crustal structures: a statistical approach based on areal distributions of pointlike features. J. Geophys. Res. Solid Earth 91 (B1), 421–434. https://doi.org/10.1029/JB091iB01p00421.

Márquez, A., Verma, S.P., Anguita, F., Oyarzun, R., Brandle, J.L., 1999. Tectonics and volcanism of Sierra Chichinautzin: extension at the front of the Central Trans-Mexican Volcanic belt. J. Volcanol. Geotherm. Res. 93 (1–2), 125–150. https://doi.org/10.1016/S0377-0273(99)00085-2.

Martí, J., López, C., Bartolini, S., Becerril, L., Geyer, A., 2016. Stress controls of monogenetic volcanism: a review. Front. Earth Sci. 4, 106. https://doi.org/10.3389/feart.2016.00106.

May, V.R., Chivas, A.R., Dosseto, A., Honda, M., Matchan, E.L., Phillips, D., Price, D.M., 2018. Quaternary volcanic evolution in the continental back-arc of southern Mendoza, Argentina. J. S. Am. Earth Sci. 84, 88–103. https://doi.org/10.1016/j.jsames.2018.02.007.

Mazzarini, F., 2004. Volcanic vent self-similar clustering and crustal thickness in the northern Main Ethiopian Rift. Geophys. Res. Lett. 31 (4) https://doi.org/10.1029/2003GL018574.

Mazzarini, F., 2007. Vent distribution and crustal thickness in stretched continental crust: the case of the Afar Depression (Ethiopia). Geosphere 3 (3), 152–162. https://doi.org/10.1130/GES00070.1.

Mazzarini, F., Ferrari, L., Isola, I., 2010. Self-similar clustering of cinder cones and crust thickness in the Michoacan–Guanajuato and Sierra de Chichinautzin volcanic fields. Trans-Mexican Volcanic Belt. Tectonophysics 486 (1–4), 55–64. https://doi.org/10.1016/j.tecto.2010.02.009.

McGee, L.E., Beier, C., Smith, I.E., Turner, S.P., 2011. Dynamics of melting beneath a small-scale basaltic system: a U-Th–Ra study from Rangitoto volcano, Auckland volcanic field, New Zealand. Contrib. Mineral. Petrol. 162 (3), 547–563. https://doi.org/10.1007/s00410-011-0611-x.

McGetchin, T.R., Settle, M., Chouet, B.A., 1974. Cinder cone growth modeled after northeast crater, Mount Etna, Sicily. J. Geophys. Res. 79 (23), 3257–3272. https://doi.org/10.1029/JB079i023p03257.

McGlashan, N., Brown, L., Kay, S., 2008. Crustal thickness in the central Andes from teleseismically recorded depth phase precursors. Geophys. J. Int. 175 (3), 1013–1022. https://doi.org/10.1111/j.1365-246X.2008.03897.x.

Moore, R.B., Clague, D.A., 1991. Geologic map of Hualalai volcano, Hawaii (no. 2213). US Geological Survey. https://doi.org/10.3133/i2213.

Morfulis, M., Báez, W., Retamoso, S., Bardelli, L., Filipovich, R., Sommer, C.A., 2020. Quantitative spatial distribution analysis of mafic monogenic volcanism in the southern Puna, Argentina: implications for magma production rates and structural control during its ascent. J. S. Am. Earth Sci. 104, 102852 https://doi.org/10.1016/j.jsames.2020.102852.

Murcia, H., Németh, K., 2020. Effusive monogenetic volcanism. In: Updates in Volcanology-Transdisciplinary Nature of Volcano Science. Intech Open. https://doi.org/10.5772/intechopen.94387.

Nche, L.A., Hasegawa, T., Aka, F.T., Kobayashi, T., Németh, K., Asaah, A.N.E., Kaneda, Y., Nishihara, A., Bate-Tibang, E.E., Lebga, A.K., Tiabou, A.F., Ngwa, C.N., Suh, C.E., 2021. Lithostratigraphy and geochemistry of Aojiki volcano and Sumiyoshiike and Yonemaru maars, Kamo Volcanic Field (Southern Kyushu), Japan. J. Volcanol. Geotherm. Res. 412, 107170 https://doi.org/10.1016/j.jvolgeores.2020.107170.

Németh, K., Kereszturi, G., 2015. Monogenetic volcanism: personal views and discussion. Int. J. Earth Sci. 104 (8), 2131–2146. https://doi.org/10.1007/s00531-015-1243-6.

Neumann van Padang, M., 1963. Catalogue of the active volcanoes and solfatara fields of Arabia and the Indian Ocean. Int. Assoc. Volcanol. Rome 16, 1–64.

Oostingh, K.F., Jourdan, F., Matchan, E.L., Phillips, D., 2017. $^{40}Ar/^{39}Ar$ geochronology reveals rapid change from plume-assisted to stress-dependent volcanism in the Newer Volcanic Province, SE Australia. Geochem. Geophys. Geosyst. 18 (3), 1065–1089. https://doi.org/10.1002/2016GC006601.
Paguican, E.M., Grosse, P., Fabbro, G.N., Kervyn, M., 2021. Morphometric classification and spatial distribution of Philippine volcanoes. J. Volcanol. Geotherm. Res. 418, 107251 https://doi.org/10.1016/j.jvolgeores.2021.107251.
Parfitt, E.A., 2004. A discussion of the mechanisms of explosive basaltic eruptions. J. Volcanol. Geotherm. Res. 134 (1–2), 77–107. https://doi.org/10.1016/j.jvolgeores.2004.01.002.
Pérez-López, R., Legrand, D., Garduño-Monroy, V.H., Rodríguez-Pascua, M.A., Giner-Robles, J.L., 2011. Scaling laws of the size-distribution of monogenetic volcanoes within the Michoacán-Guanajuato Volcanic Field (Mexico). J. Volcanol. Geotherm. Res. 201 (1–4), 65–72. https://doi.org/10.1016/j.jvolgeores.2010.09.006.
Philip, H., Avagyan, A., Karakhanian, A., Ritz, J.F., Rebai, S., 2001. Estimating slip rates and recurrence intervals for strong earthquakes along an intracontinental fault: example of the Pambak-Sevan-Sunik fault (Armenia). Tectonophysics 343 (3–4), 205–232. https://doi.org/10.1016/S0040-1951(01)00258-X.
Pioli, L., Erlund, E., Johnson, E., Cashman, K., Wallace, P., Rosi, M., Granados, H.D., 2008. Explosive dynamics of violent Strombolian eruptions: the eruption of Parícutin Volcano 1943-1952 (Mexico). Earth Planet. Sci. Lett. 271 (1–4), 359–368. https://doi.org/10.1016/j.epsl.2008.04.026.
Pioli, L., Azzopardi, B.J., Cashman, K.V., 2009. Controls on the explosivity of scoria cone eruptions: magma segregation at conduit junctions. J. Volcanol. Geotherm. Res. 186 (3–4), 407–415. https://doi.org/10.1016/j.jvolgeores.2009.07.014.
Ponomareva, V.V., Churikova, T., Melekestsev, I.V., Braitseva, O.A., Pevzner, M., Sulerzhitskii, L., 2007. Late pleistocene-holocene volcanism on the Kamchatka peninsula, northwest pacific region. In: Eichelberger, J., Gordeev, E., Kasahara, M., Izbekov, P., Lees, J. (Eds.), Volcanism and Tectonics of the Kamchatka Peninsula and Adjacent Arcs, American Geophysical Union Geophysical Monograph Series, vol. 172, pp. 165–198.
Porter, S.C., 1972. Distribution, morphology, and size frequency of cinder cones on Mauna Kea volcano, Hawaii. Geol. Soc. Am. Bull. 83 (12), 3607–3612. https://doi.org/10.1130/0016-7606(1972)83[3607:DMASFO]2.0.CO;2.
Riedel, C., Ernst, G.G.J., Riley, M., 2003. Controls on the growth and geometry of pyroclastic constructs. J. Volcanol. Geotherm. Res. 127 (1–2), 121–152. https://doi.org/10.1016/S0377-0273(03)00196-3.
Risica, G., Di Roberto, A., Speranza, F., Del Carlo, P., Pompilio, M., Meletlidis, S., Rosi, M., 2020. Refining the Holocene eruptive activity at Tenerife (Canary Islands): the contribution of palaeomagnetism. J. Volcanol. Geotherm. Res. 401, 106930 https://doi.org/10.1016/j.jvolgeores.2020.106930.
Risse, A., Trumbull, R.B., Coira, B., Kay, S.M., van den Bogaard, P., 2008. $^{40}Ar/^{39}Ar$ geochronology of mafic volcanism in the back-arc region of the southern Puna plateau, Argentina. J. S. Am. Earth Sci. 26 (1), 1–15. https://doi.org/10.1016/j.jsames.2008.03.002.
Roggensack, K., 2001. Sizing up crystals and their melt inclusions: a new approach to crystallization studies. Earth Planet. Sci. Lett. 187 (1–2), 221–237. https://doi.org/10.1016/S0012-821X(01)00269-2.
Romero, J.E., Burton, M., Cáceres, F., Taddeucci, J., Civico, R., Ricci, T., Pankhurst, M.J., Hernández, P.A., Bonadonna, C., Llewellin, E.W., Pistolesi, M., 2022. The initial phase of the 2021 Cumbre Vieja ridge eruption (Canary Islands): products and dynamics controlling edifice growth and collapse. J. Volcanol. Geotherm. Res. 431, 107642 https://doi.org/10.1016/j.jvolgeores.2022.107642.
Runge, M.G., Bebbington, M.S., Cronin, S.J., Lindsay, J.M., Moufti, M.R., 2015. Sensitivity to volcanic field boundary. J. Appl. Volcanol. 4 (1), 1–18. https://doi.org/10.1186/s13617-015-0040-z.
Schaaf, P., Stimac, J.I.M., Siebe, C., Macías, J.L., 2005. Geochemical evidence for mantle origin and crustal processes in volcanic rocks from Popocatépetl and surrounding monogenetic volcanoes, central Mexico. J. Petrol. 46 (6), 1243–1282. https://doi.org/10.1093/petrology/egi015.
Schmidt, C., Laag, C., Whitehead, M., Profe, J., Aka, F.T., Hasegawa, T., Kereszturi, G., 2022. The complexities of assessing volcanic hazards along the Cameroon Volcanic Line using spatial distribution of monogenetic volcanoes. J. Volcanol. Geotherm. Res. 427, 107558 https://doi.org/10.1016/j.jvolgeores.2022.107558.
Schober, P., Boer, C., Schwarte, L.A., 2018. Correlation coefficients: appropriate use and interpretation. Anesth. Analg. 126 (5), 1763–1768. https://doi.org/10.1213/ANE.0000000000002864.
Schulte-Pelkum, V., Biasi, G., Sheehan, A., Jones, C., 2011. Differential motion between upper crust and lithospheric mantle in the central Basin and Range. Nat. Geosci. 4 (9), 619–623. https://doi.org/10.1038/ngeo1229.
Scoon, R.N., Scoon, R.N., van Steenbergen, 2018. Geology of National Parks of Central/Southern Kenya and Northern Tanzania. Springer, Cham.
Sieron, K., Guilbaud, M.N., Zarazúa-Carbajal, M.C., Juárez Cerrillo, S.F., 2023. Monogenetic volcanism in subduction settings: comparative statistical study of the Sierra Chichinautzin and Los Tuxtlas Volcanic Fields in Mexico. Bull. Volcanol. 85 (2), 14. https://doi.org/10.1007/s00445-023-01625-4.
Sigurdsson, H., Houghton, B., McNutt, S., Rymer, H., Stix, J. (Eds.), 2015. The Encyclopedia of Volcanoes. Elsevier.
Søager, N., Holm, P.M., Llambías, E.J., 2013. Payenia volcanic province, southern Mendoza, Argentina: OIB mantle upwelling in a backarc environment. Chem. Geol. 349, 36–53. https://doi.org/10.1016/j.chemgeo.2013.04.007.
Späth, A., Le Roex, A.P., Opiyo-Akech, N., 2000. The petrology of the Chyulu Hills volcanic province, southern Kenya. J. Afr. Earth Sci. 31 (2), 337–358. https://doi.org/10.1016/S0899-5362(00)00092-0.
Stanley, W.D., Mooney, W.D., Fuis, G.S., 1990. Deep crustal structure of the Cascade Range and surrounding regions from seismic refraction and magnetotelluric data. J. Geophys. Res. Solid Earth 95 (B12), 19419–19438. https://doi.org/10.1029/JB095iB12p19419.
Tadono, T., Nagai, H., Ishida, H., Oda, F., Naito, S., Minakawa, K., Iwamoto, H., 2016. Generation of the 30 m-mesh global Digital Surface Model by ALOS PRISM. Int. Arch. Photogramm. Remote. Sens. Spat. Inf. Sci. XLI-B4, 157–162. https://doi.org/10.5194/isprsarchives-XLI-B4-157-2016.
Tanaka, K.L., Shoemaker, E.M., Ulrich, G.E., Wolfe, E.W., 1986. Migration of volcanism in the San Francisco volcanic field, Arizona. Geol. Soc. Am. Bull. 97 (2), 129–141. https://doi.org/10.1130/0016-7606(1986)97<129:MOVITS>2.0.CO;2.
Tang, Z., Julià, J., Zahran, H., Mai, P.M., 2016. The lithospheric shear-wave velocity structure of Saudi Arabia: young volcanism in an old shield. Tectonophysics 680, 8–27. https://doi.org/10.1016/j.tecto.2016.05.004.
Tao, K., Niu, F., Ning, J., Chen, Y.J., Grand, S., Kawakatsu, H., Tanaka, S., Obayashi, M., Ni, J., 2014. Crustal structure beneath NE China imaged by NECESSArray receiver function data. Earth Planet. Sci. Lett. 398, 48–57. https://doi.org/10.1016/j.epsl.2014.04.043.
Tatsumi, Y., 1989. Migration of fluid phases and genesis of basalt magmas in subduction zones. J. Geophys. Res. Solid Earth 94 (B4), 4697–4707. https://doi.org/10.1029/JB094iB04p04697.
Teklay, M., Scherer, E.E., Mezger, K., Danyushevsky, L., 2010. Geochemical characteristics and Sr-Nd-Hf isotope compositions of mantle xenoliths and host basalts from Assab, Eritrea: implications for the composition and thermal structure of the lithosphere beneath the Afar Depression. Contrib. Mineral. Petrol. 159 (5), 731–751. https://doi.org/10.1007/s00410-009-0451-0.
Tezel, T., Shibutani, T., Kaypak, B., 2013. Crustal thickness of Turkey determined by receiver function. J. Asian Earth Sci. 75, 36–45. https://doi.org/10.1016/j.jseaes.2013.06.016.
Thomson, B.J., Lang, N.P., 2016. Volcanic edifice alignment detection software in MATLAB: Test data and preliminary results for shield fields on Venus. Comput. Geosci. 93, 1–11. https://doi.org/10.1016/j.cageo.2016.04.012.
USGS., n.d. Davis Lake Volcanic Field. https://www.usgs.gov/volcanoes/davis-lake-volcanic-field (accessed on 05 August 2022).
Uslular, G., Le Corvec, N., Mazzarini, F., Legrand, D., Gençalioğlu-Kuşcu, G., 2021. Morphological and multivariate statistical analysis of quaternary monogenetic vents in the Central Anatolian Volcanic Province (Turkey): Implications for the volcano-tectonic evolution. J. Volcanol. Geotherm. Res. 416, 107280 https://doi.org/10.1016/j.jvolgeores.2021.107280.
Valentine, G.A., Connor, C.B., 2015. Basaltic volcanic fields. In: Sigurdsson, H., Houghton, B., McNutt, S., Rymer, H., Stix, J. (Eds.), The Encyclopedia of Volcanoes. Academic Press, pp. 423–439.
Valentine, G.A., Krogh, K.E., 2006. Emplacement of shallow dikes and sills beneath a small basaltic volcanic center-the role of pre-existing structure (Paiute Ridge, southern Nevada, USA). Earth Planet. Sci. Lett. 246 (3–4), 217–230. https://doi.org/10.1016/j.epsl.2006.04.031.
Valentine, G.A., Perry, F.V., 2007. Tectonically controlled, time-predictable basaltic volcanism from a lithospheric mantle source (central Basin and Range Province, USA). Earth Planet. Sci. Lett. 261 (1–2), 201–216. https://doi.org/10.1016/j.epsl.2007.06.029.
Valentine, G.A., Krier, D.J., Perry, F.V., Heiken, G., 2007. Eruptive and geomorphic processes at the Lathrop Wells scoria cone volcano. J. Volcanol. Geotherm. Res. 161 (1–2), 57–80. https://doi.org/10.1016/j.jvolgeores.2006.11.003.
van den Hove, J., Grose, L., Betts, P.G., Ailleres, L., Van Otterloo, J., Cas, R.A., 2017. Spatial analysis of an intra-plate basaltic volcanic field in a compressional tectonic setting: south-eastern Australia. J. Volcanol. Geotherm. Res. 335, 35–53. https://doi.org/10.1016/j.jvolgeores.2017.02.001.
Villamor, P., Berryman, K.R., Ellis, S.M., Schreurs, G., Wallace, L.M., Leonard, G.S., Langridge, R.M., Ries, W.F., 2017. Rapid evolution of subduction-related continental intraarc rifts: the Taupo Rift, New Zealand. Tectonics 36 (10), 2250–2272. https://doi.org/10.1002/2017TC004715.
Wallace, P.J., Carmichael, I.S., 1999. Quaternary volcanism near the Valley of Mexico: implications for subduction zone magmatism and the effects of crustal thickness variations on primitive magma compositions. Contrib. Mineral. Petrol. 135 (4), 291–314. https://doi.org/10.1007/s004100050513.
Wallace, P.J., Plank, T., Edmonds, M., Hauri, E.H., 2015. Volatiles in magmas. In: Sigurdsson, H., Houghton, B., McNutt, S., Rymer, H., Stix, J. (Eds.), The Encyclopedia of Volcanoes. Academic Press, pp. 423–439.
Weller, J.N., Martin, A.J., Connor, C.B., Connor, L.J., Karakhanian, A., 2006. Modelling the spatial distribution of volcanoes: an example from Armenia. Stat. Volcanol. 1, 77–88.
Wollschlaeger, D., 2022. Package 'shotGroups'. https://cran.r-project.org/web/packages/shotGroups/shotGroups.pdf (Accessed 05 November 2022).
Wood, C.A., 1979. Monogenetic volcanoes of the terrestrial planets. In: Proc. Lunar Planet. Sci. Conf. 10th (1979), pp. 2815–2840.
Wood, C.A., 1980. Morphometric evolution of cinder cones. J. Volcanol. Geotherm. Res. 7 (3–4), 387–413. https://doi.org/10.1016/0377-0273(80)90040-2.
Yacouba, I.A., Glaznev, V.N., 2021. The thickness of the Earth's crust in the territory of Republic of the Niger according to the stochastic interpretation of the gravity field. In: Kukkonen, I.T., Veikkolainen, T., Heinonen, S., Karell, F., Kozlovskaya, E., Luttinen, A., Nikkilä, K., Nykänen, V., Poutanen, M., Skyttä, P., Tanskanen, E., Tiira, T. (Eds.), Lithosphere 2021 – Eleventh Symposium on the Structure, Composition and Evolution of the Lithosphere in Finland. Program and Extended Abstracts, January 19–20, 2021, Institute of Seismology, University of Helsinki. Report S-71, pp. 157–160.
Yu, F., Yuan, W., Han, S., Ma, Z., Jin, K., 2004. Chronological and geochemical feature and degassing evaluation of volcano at Dayizishan, Jilin province. Acta Geoscien. Tica Sin. Ica. 25 (2), 219–223 (in Chinese).

Yu, F., Han, S., Ma, Z., Xie, R., 2005. Uranium series chronology of the Late Pleistocene basalt from the Longgang volcanoes, Jilin Province. Acta Geol. Sin. Engl. Edn. 79 (2), 211–214. https://doi.org/10.1111/j.1755-6724.2005.tb00883.x.

Zandt, G., Leidig, M., Chmielowski, J., Baumont, D., Yuan, X., 2003. Seismic detection and characterization of the Altiplano-Puna magma body, central Andes. Pure Appl. Geophys. 160, 789–807. https://doi.org/10.1007/PL00012557.

Zhang, R., Kereszturi, G., Brenna, M., Ahn, U.S., 2022. Sensitivity assessment of morphometric parameters of monogenetic volcanic landforms with global free DEMs. Geomorphology 108408. https://doi.org/10.1016/j.geomorph.2022.108408.

Zhao, Y.W., Li, N., Fan, Q.C., Zou, H., Xu, Y.G., 2014. Two episodes of volcanism in the Wudalianchi volcanic belt, NE China: evidence for tectonic controls on volcanic activities. J. Volcanol. Geotherm. Res. 285, 170–179. https://doi.org/10.1016/j.jvolgeores.2014.08.016.

Zhao, B., Xu, D., Bai, Z., Chen, Z., 2021. Volcanism in the Longgang volcanic field of NE China: insights from eruption history, volcano types and geochemical characteristics. Geol. Soc. Lond. Spec. Publ. 510 (1), 27–39. https://doi.org/10.1144/SP510-2020-60.